

Performance of Wicking Geotextile on Mitigating Water Pumping Issue on I-44 Highway



March 2020
Final Report

Project number TR201905
MoDOT Research Report number cmr 20-003

PREPARED BY:

Xiong Zhang, Ph.D., PE.

Javad Galinmoghadam, M.Sc.

Missouri University of Science and Technology

PREPARED FOR:

Missouri Department of Transportation

Construction and Materials Division, Research Section

TECHNICAL REPORT DOCUMENTATION PAGE

1. Report No. cmr 20-003	2. Government Accession No.	3. Recipient's Catalog No.	
4. Title and Subtitle Performance of Wicking Geotextile on Mitigating Water Pumping Issue on I-44 Highway		5. Report Date January 2020 Published: March 2020	
		6. Performing Organization Code	
7. Author(s) Xiong Zhang, Ph.D., PE. Javad Galinmoghadam, M.Sc. https://orcid.org/0000-0002-2787-4918		8. Performing Organization Report No.	
9. Performing Organization Name and Address Department of Civil, Architectural and Environmental Engineering Missouri University of Science and Technology 1401 N. Pine St., Rolla, MO 65409		10. Work Unit No.	
		11. Contract or Grant No. MoDOT project # TR201905	
12. Sponsoring Agency Name and Address Missouri Department of Transportation (SPR-B) Construction and Materials Division P.O. Box 270 Jefferson City, MO 65102		13. Type of Report and Period Covered Final Report (September 2018-November 2019)	
		14. Sponsoring Agency Code	
15. Supplementary Notes Conducted in cooperation with the U.S. Department of Transportation, Federal Highway Administration. MoDOT research reports are available in the Innovation Library at https://www.modot.org/research-publications .			
16. Abstract Water within pavement layers is the major cause of pavement distresses. An increase in pore water pressure caused by traffic loads causes fine particles of subgrade and subbase to migrate to base course layer. This migration results in the formation of void spaces and reduction in support of the pavement. On the other hand, migrated fines may clog the granular base course and reduce its drainage. All of these negative effects would reduce the durability of the pavement and damage it. In this study, a full-scale test section located along I-44 highway was constructed and monitored to investigate the effect of a new type of wicking geotextile to enhance pavement drainage and to mitigate water pumping. Analyzing one year of data acquired from the sensors shows that the wicking geotextile has successfully reduced the volumetric water content of the base course material up to 5%-10% and enhanced the pavement drainage capacity. This conclusion has been verified by a set of small scale box tests in the laboratory as well. Observations showed that the efficiency of wicking geotextile is considerably better than conventional drainage systems including French drains when the pavement is under unsaturated condition.			
17. Key Words Pavement pumping; Drainage; Unsaturated soils, H2Ri wicking geotextile		18. Distribution Statement No restrictions. This document is available through the National Technical Information Service, Springfield, VA 22161.	
19. Security Classif. (of this report) Unclassified.	20. Security Classif. (of this page) Unclassified.	21. No. of Pages 64	22. Price

**PERFORMANCE OF WICKING GEOTEXTILE ON MITIGATING
WATER PUMPING ISSUE ON I-44 HIGHWAY**

by

Javad Galinmoghadam

Graduate Student

Department of Civil, Architectural and Environmental Engineering
Missouri University of Science and Technology

Project Lead

Xiong Zhang, Ph.D., P.E.

Associate Professor,

Department of Civil, Architectural and Environmental Engineering
Missouri University of Science and Technology

Project Title: Use of H2Ri to Mitigate Pumping in Concrete Pavement Shoulders

Performed in cooperation with
TENCATE GEOSYNTHETICS (North America)
and
Missouri Department of Transportation

January 2020

COPYRIGHT

Authors herein are responsible for the authenticity of their materials and for obtaining written permissions from publishers or individuals who own the copyright to any previously published or copyrighted material used herein.

DISCLAIMER

This document is disseminated under the sponsorship of the Missouri Department of Transportation in the interest of information exchange. The Missouri Government assumes no liability for the use of the information contained in this document. The Missouri Government does not endorse products or manufacturers. Trademarks or manufacturers' names appear in this report only because they are considered essential to the objective of the document.

Opinions and conclusions expressed or implied in the report are those of the author(s). They are not necessarily those of the funding agencies. This report does not constitute a standard, specification, or regulation.

ACKNOWLEDGMENTS

The author wishes to express their appreciation to the Missouri Department of Transportation (MODOT) for sponsoring this research project and TENCATE GEOSYNTHETICS (North America) for donating the wicking geotextile needed for this research. The research team would like to avail this opportunity to wholeheartedly thank Mr. John P. Donahue, Construction and Materials Liaison Engineer, Mr. Bill Stone, former Research Administrator, and Christopher Graham, Resident Engineer of MODOT for their great help and support during the process. Without their help, this study would have been impossible. Many graduate students in the Geotechnical Group at Missouri S&T helped the fieldwork including Chuang Lin, Yipeng Guo, Beshoy Riad, Shanmei Li, Donggen Chen, Anyou Zhu, and Xinxing Zhou. Their help during the process is highly appreciated as well.

EXECUTIVE SUMMARY

A new type of wicking geotextile was used to mitigate pumping in pavement systems. This type of wicking geotextile was found to be useful in draining water from the soils in the pavement and reducing the risk of generating positive pore pressure that induces pumping. Three test sections on the shoulder of I-44 Highway in Missouri were constructed and instrumented. The construction of the test section finished in September 2018. In total 33 volumetric water content sensors were placed in the three test sections. Two of these sections were treated by placing one layer of wicking geotextile on top of a clayey subgrade at the road shoulder. One control section without wicking geotextile was instrumented in order to make a comparison between improved and unimproved design sections.

The most recent data was collected from the data logger installed at the test location on October 03, 2019. Over one year of monitoring period, all of the 33 sensors are working and transmitting volumetric water content and temperature data from different locations under the shoulder pavement. Results obtained from field sections show that the improvement in pavement drainage is significant due to the installation of wicking geotextile. Along with the field test sections, laboratory studies were done to acquire a deeper understanding of the efficiency of the wicking geotextile in draining water out of the soil. The results of the laboratory investigations were consistent with field observations.

TABLE OF CONTENTS

COPYRIGHT.....	iii
DISCLAIMER.....	iii
ACKNOWLEDGMENTS.....	iii
EXECUTIVE SUMMARY.....	iv
TABLE OF CONTENTS.....	v
LIST OF FIGURES.....	vii
CHAPTER 1: INTRODUCTION.....	1
1.1 Problem Statement.....	1
1.2 Background.....	2
1.3 A New Wicking Geotextile.....	4
1.4 Organization.....	6
CHAPTER 2: TEST DESIGN AND CONSTRUCTION PROCESS.....	7
2.1 Design.....	7
2.2 Sensor Specifications.....	9
2.3 Construction of Test Sections.....	9
2.4 3D Reconstruction of the Test Site.....	17
CHAPTER 3: PRELIMINARY RESULTS.....	19
3.1 Introduction.....	19
3.2 Local Climatic Conditions.....	19
3.3 Volumetric Water Content at Different Sections.....	22
3.4 VWC at Different Elevations of Each Section.....	25
3.5 VWCs at the Critical Locations for Pumping.....	29
3.6 Contour Plots of Volumetric Water Content at Different Times.....	31
CHAPTER 4: COMPLIMENTARY TESTS.....	37
4.1 Particle Size Distribution Test.....	37
4.2 Briaud Compaction Test.....	37
4.3 Proctor Compaction Tests.....	38
4.4 Laboratory Hydraulic Conductivity Test.....	39
CHAPTER 5: SMALL SCALE BOX TEST.....	40
5.1 Experimental Setup.....	40
5.2 Instrumentation.....	40

5.3 Experimental Design	42
5.4 Test Procedures.....	43
5.5 Results and Discussions.....	43
CHAPTER 6: CONCLUSION	51
REFERENCES	53

LIST OF FIGURES

Figure 1.1 Damage caused by water pumping at the inner edge of the road shoulder	1
Figure 1.2 Schematics of pumping action.....	3
Figure 1.3 Wicking geotextile. a) geotextile photo, b) schematics of geotextile cross-section, c) schematics of a single wicking yarn, d) schematics of wicking geotextile working mechanism...	5
Figure 2.1 Aerial photo of the proposed testing site	7
Figure 2.2 Schematic plot of test section design.....	8
Figure 2.3 CS650 Water Content Reflectometer	9
Figure 2.4 View of the site before construction.....	10
Figure 2.5 Off-shoulder work	10
Figure 2.6 View of the shoulder after excavation	11
Figure 2.7 Sensor installation in the subgrade soil	12
Figure 2.8 L-shaped placement of wicking geotextile in Section 1	12
Figure 2.9 Horizontal placement of wicking geotextile in test section 2.....	13
Figure 2.10 Sensor installation above the wicking geotextile in test section 2	13
Figure 2.11 Compaction of the base course	14
Figure 2.12 Preparing a trench for sensor installation using a trench-digger	15
Figure 2.13 View of the test site after construction	15
Figure 2.14 Location of the test sections after paving the road shoulder	16
Figure 2.15 The final configuration of the test site.....	16
Figure 2.16 Exposing the outer end of the wicking geotextile on February 9, 2019.....	17
Figure 2.17 Scan data after excavation to the depth of 18in.....	17
Figure 2.18 Scan data after paving the shoulder	18
Figure 2.19 The final constructed cross-section	18
Figure 2.20 Site overview after construction	18
Figure 3.1 Relative locations of two closest weather stations to the test site	19
Figure 3.2 General climatic information based on data obtained from a weather station at Camdenton, Missouri. a) Total solar radiation, b) Mean wind speed, c) Mean air temperature, d) Relative humidity, e) Precipitation and potential evapotranspiration, f) Air suction.	22
Figure 3.3 VWC at the outer edge of the subgrade.....	22
Figure 3.4 Relative VWC in different test sections at the top of the base course and the inner edge of the base course	24
Figure 3.5 Relative VWC in the subgrade at the edge of the driving lane.	25

Figure 3.6 Variation of VWC in the control section at different elevations at the inner edge of the shoulder.....	26
Figure 3.7 Variation of VWC in the control section at different elevations at the middle of the shoulder.....	27
Figure 3.8 Variation of VWC in section 1 at different elevations at the inner edge of the shoulder.....	28
Figure 3.9 Variations of VWC at sensors 12, 15, and 19 in section 1 in the middle of the shoulder.....	28
Figure 3.10 Variation of VWC in section 1 at different elevations at the outer edge of the shoulder.....	29
Figure 3.11 Variation of VWC in section 2 at different elevations at the inner edge of the shoulder.....	30
Figure 3.12 Variation of VWC in section 2 at different elevations at the middle of the shoulder.....	30
Figure 3.13 Variation of VWC in section 2 at different elevations at the outer edge of the shoulder.....	30
Figure 3.14 Variations of VWC at different elevations at the inner edge of the shoulder	31
Figure 3.15 VWC at different times before February 9, 2019.....	33
Figure 3.16 VWC at different times after February 9, 2019.....	35
Figure 4.1 Particle size distribution of the base course material passing 3/8in. sieve.....	37
Figure 4.2 BCD field test.....	38
Figure 4.3 Correlation of BCD modulus with soil density for the base course material.....	38
Figure 4.4 Compaction test results.....	39
Figure 5.1 Test apparatus.....	42
Figure 5.2 Test setup for four different cases and typical sensor arrangement. Case I: control case with no drainage, Case II: Horizontal wicking geotextile, Case III: L shaped wicking geotextile, Case IV: French drain. (dimensions in inches).....	42
Figure 5.3 Average VWC for different cases.	45
Figure 5.4 Normalized average VWC for different cases at top sensors (h = 15.4 in).....	46
Figure 5.5 Distributions of VWC in all four cases at initial condition (VWC in percentage).....	47
Figure 5.6 Distributions of VWC in all four cases after 3 hours (VWC in percentage).....	48
Figure 5.7 Distributions of VWC in all four cases after 2 days (VWC in percentage).....	48
Figure 5.8 Relative VWC after 2 days.	50

CHAPTER 1: INTRODUCTION

1.1 Problem Statement

Pumping is the ejection of water and fine materials out of the pavement under pressure (i.e., traffic loads) through cracks. The water ejection, carrying fine materials, may result in progressive material deterioration and loss of support. Evidence of pumping includes surface stains and accumulated material on the road surface close to joints and cracks (please see Figure 1.1).



Figure 1.1 Damage caused by water pumping at the inner edge of the road shoulder

Pumping is influenced by several factors: joints and cracks, heavy axle loads, unsuitable subgrade soil, and “free” water. Heavy axle loads deflect the pavement and increase pore water pressure. The “free” water, together with the fine materials, is then forced to squeeze out under heavy axle loads through joints and cracks. The repeated loading increases pore pressure and fines migration, thus, the pavement gradually loses support. As the fine materials are pumped out, the voids of the base course enlarge and more “free” water accumulates near the joints and cracks during rainfall events. In turn, more fine materials are pumped out and the subsurface layers and the pavement eventually deteriorates due to lack of support from the lower layers. Therefore, if the amount of water (both “free” water and capillary water) within the base course can be controlled at a relatively lower range (unsaturated condition), the fines within the base

and subgrade will not be pumped out, and the overall pavement performance is expected to improve.

In recent years, a new type of wicking geotextile has been developed to remove the excess water in the pavement structure and potentially maintain good pavement performance and longevity. The wicking geotextile is made of a special type of hydrophilic Nylon fibers with multichannel cross-sections. The multichannel cross-section has a high shape factor and a number of channels per fiber, which give wicking geotextile great potential for maximizing capillary action and water transport in an unsaturated environment.

By installing a layer of wicking geotextile horizontally beneath the road shoulder, the excess water in the pavement structure can be absorbed from the soils, transported along the wicking geotextile to the slopes, and vaporized to the surrounding atmosphere. It is likely to generate a relatively dry zone in the pavement structure which can help mitigate pumping, thus improve the overall pavement performance. A test site was built to investigate the use of wicking geotextile to mitigate pumping damage, which is located at milepost 117.2 of Eastbound Interstate 44 near Phillipsburg, Missouri (Latitude: 37.551983°, Longitude: -92.801741°). This report presents the performance of the test site during the monitoring period from October 2018 to October 2019.

1.2 Background

Pumping is an issue causing failure in both rigid and flexible pavements. This type of failure is caused by either ejection of water and fine contents through pavements joints, cracks, and edges or redistribution of materials underneath the slab. Three conditions are required for pumping to occur: (a) large deflection (heavy axle loads and/or thin slabs); (b) water in the pavement; and (c) materials that are susceptible to pumping. The schematic view of the pumping problem is shown in Figure 1.2 . Deformation under heavy wheel loads generates excess pore water pressure in a saturated base course layer. The pore water pressure is typically generated at top of a layer that contains higher fines content mainly for two reasons. First, this layer can hold more water and due to less permeability, and infiltrated water can pond on top of it. Second, due to less permeability, the loading applied is close to undrained condition. Thus, repeated traffic loads increase pore water pressure. Eventually, the excess pore water pressure is high enough to cause water flow and displace small particles in the soil layer. This results in emerging void spaces due to displaced soil particles (Holtz 2008). As time passes, these void spaces get larger and result in a lack of support and bearing capacity failure for the upper pavement layer (Al-Qadi et al. 2004, Zuo et al. 2004, Diefenderfer 2005). On the other hand, the displaced particles move to the upper layer which initially had no fines and a higher permeability (Kermani et al. 2018a). Fines migration changes Grain Size Distribution of the upper layer, decreasing its permeability, increasing capillary height, and increasing soil water storage in unsaturated condition. The latter also results in a smaller modulus value for this layer. Eventually, this process causes cracks at the pavement surface resulting in more water infiltration and more damage. At extreme conditions, fine particles along with water are ejected through the cracks of the pavement surface. By this time, all of the pavement layers have been affected by the pumping and the overall performance of the pavement has significantly reduced.

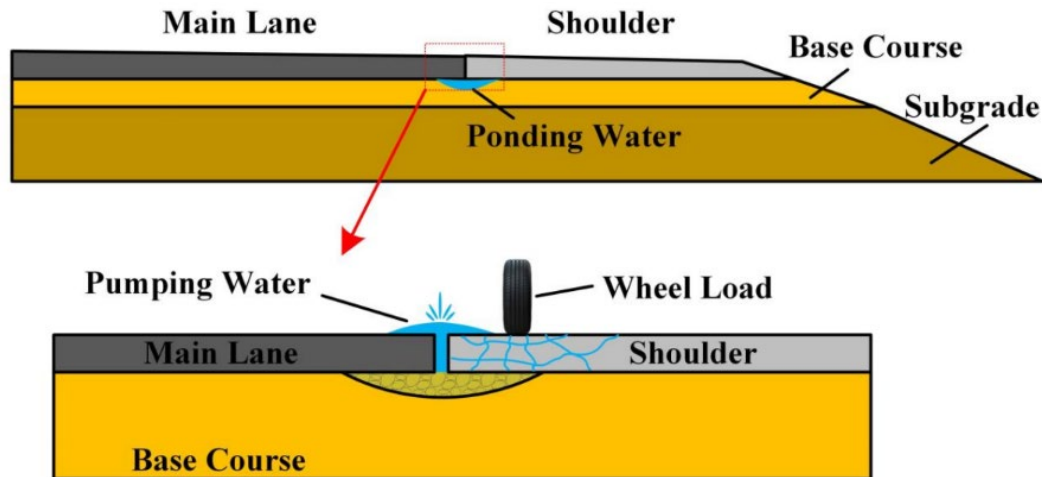


Figure 1.2 Schematics of pumping action

Pumping has been a problem since the 1940s with the increase of traffic loads during World War II. Pumping can reduce the life of the pavement, increase maintenance costs, and affect the safety of the road. It has been shown in many studies that the migration of fine particles into pavement upper layer can significantly change the properties of the layers including moduli, permeability, gradation, and soil classification (Holtz et al. 2008, Christopher et al. 2010). The detrimental effect of pumping may increase due to inadequate compaction during construction or poor mix design, high water table and poor drainage (Tosti and Benedetto 2012).

The generation of excess pore water pressure under cyclic loading has been studied by many researchers. It was reported that the cyclic wheel load can generate excess pore water pressure up to 28 kPa (Alobaidi and Hoare 1996, Huang et al. 2018, Zuo et al. 2004) and a water velocity of up to 1 m/s (Hansen et al. 1991). Dempsey (1982), based on field and experiment results, pointed out that a pore pressure increase of 20 kPa is enough to easily move finer grains (particles having a size <10 mm). On the other hand, if we can reduce the moisture content in the soils and subsequently the maximum excess pore water pressure generated during the repeated traffic loading, it is expected that the pumping issue can be mitigated.

Early attempts to eliminate pumping included replacement of the contaminated granular base between the slab and the subgrade with better base course materials and stabilizing subbase. The latter procedure has been used since the 1950s by using lean concrete or asphalt concrete (Van Wijk and Lovell 1986).

Using geotextile is another common treatment to mitigate pumping which has been studied by several researchers (Snaith and Bell 1978, Grau 1984, Ayres 1986, Yang and Yu 1989, DeBerardino and Baldwin 1996, Black and Holtz 2002, Collins et al. 2005, Hufenus et al. 2006, Loulizi et al. 2007, Chapuis et al. 2008, Han 2013, Abu-Farsakh et al. 2016, Huang et al. 2018). The major contribution of geotextile in mitigating pumping issues is taking advantage of its separation and filtration functions. By adding a layer of geotextile to the pavement structure, the overall moduli of soil-geotextile composite could be improved. However, the increase in pavement section moduli is more significant in the first several months after construction when geotextile is used as a separator (Collins et al. 2005), especially when the fill layer above the

geotextile is thin and the subgrade is weak. One limitation of installing geotextile as a separator is the potential clogging due to pumping which has been frequently discussed in literature. Several researchers developed criteria for geotextile used as a separator, based on its opening size and the particle size distribution of the underlying soil (Alobaidi and Hoare 1998, Grau 1984, Black and Holtz 2002, Chapuis et al. 2008, Koerner and Koerner 2015, Miskowska et al. 2017, Kermani et al. 2018b).

Geogrids were often used to provide additional reinforcement. The load was redistributed with less concentration beneath the tire, resulting in less deformation and lower pore water pressure under repeated traffic loads. (Al-Qadi et al. 1994, Abu-Farsakh et al. 2016). Using geogrid was also found to be effective in mitigating pumping but less significant than geotextile (Hufenus et al. 2006, Loulizi et al. 2007, Abu-Farsakh et al. 2016, Huang et al. 2018).

As an alternative treatment, controlling and draining water within the pavement structure has not been studied extensively. A commonly used pavement drainage system is the open-graded base course (Xiao et al. 2014). Diefenderfer et al. (2005) mentioned that subsurface drainage can increase the structural number and the service life of the pavement up to 44%. Providing sufficient drainage is important in mitigating pumping issues within a pavement structure. However, pumping induced clogging in the long term is an issue and the use of a geotextile separator is advised (DeBerardino and Baldwin 1996). It has been found that conventional drainage systems rely on gravity to drain free water out of the pavement and thus cannot drain capillary water (Lin and Zhang 2018a). Under repeated loading, pore water pressure in the pavement can increase to a positive value even when the pavement was initially under unsaturated conditions as mentioned previously (Hansen et al. 1991, Dempsey 1982).

1.3 A New Wicking Geotextile

In recent years, a new type of wicking geotextile has been developed that is able to remove both capillary water and gravitational (free) water out of the pavement structure in an effort to maintain good pavement performance and longevity. Figure 1.3a shows a picture of the new wicking geotextile. The schematic cross-section of the wicking geotextile is illustrated in Figure 1.3b. As depicted in Figures 1.3a and 1.3b, the wicking geotextile has two different warp yarns which are woven together by wefts of other geosynthetics material. The reinforcing warp yarn is made of polypropylene with high tensile strength. The wicking yarn consists of 144 wicking warps for drainage purposes. As can be seen, wicking yarns are weaved at the top, middle, and bottom of the geotextile cross-section allowing the wicking geotextile to absorb water from both the top and the bottom surface. The unique properties of the wicking geotextile come from the hydrophilic and hygroscopic nylon filaments with a unique multi-channel cross-section as shown in Figure 1c. Each wicking warp has an average diameter of 30-50 μm and an average groove width of 5-12 μm . The multichannel cross-section has a high shape factor and a great number of channels per fiber (specific surface area = 3650 cm^2/g), which give the wicking geotextile great potential for maximizing capillary action and water transport in an unsaturated condition. Figure 1.3d shows the mechanism of the wicking geotextile to drain water, which will be explained in the following section.

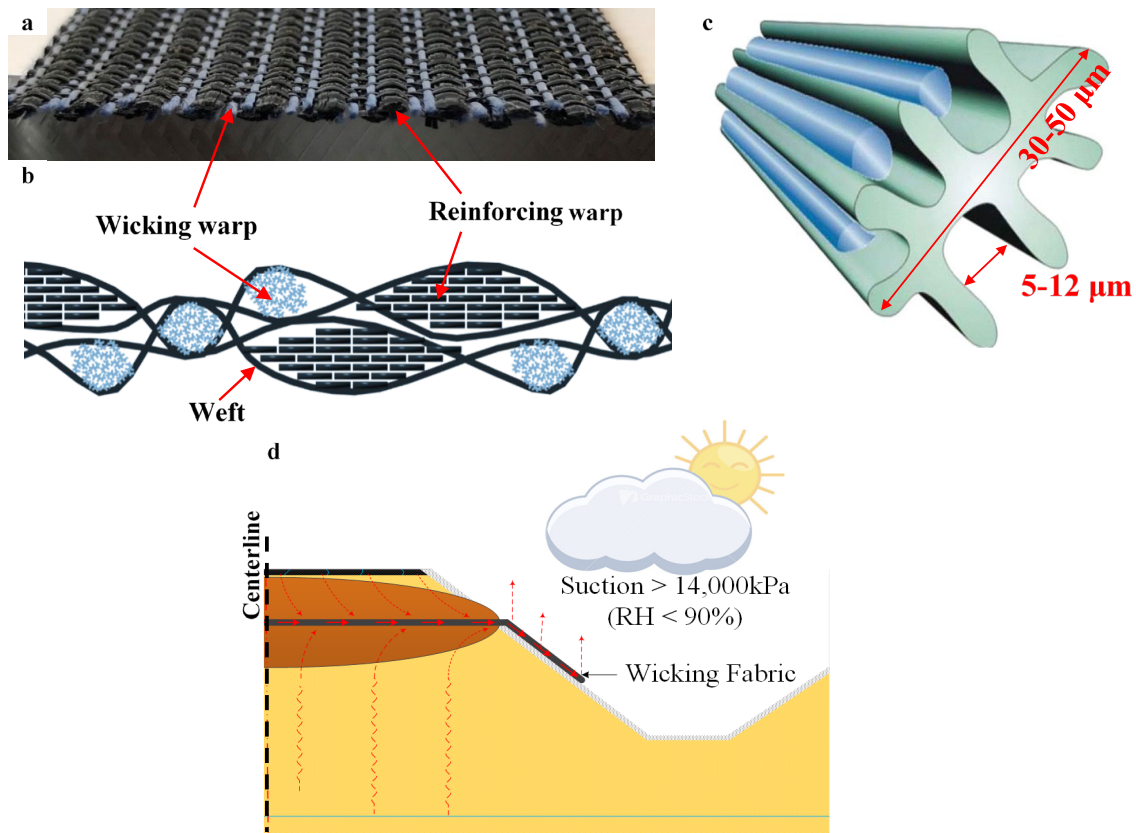


Figure 1.3 Wicking geotextile. a) geotextile photo, b) schematics of geotextile cross-section, c) schematics of a single wicking yarn, d) schematics of wicking geotextile working mechanism

As mentioned above, the weaving pattern of the wicking yarns in the wicking geotextile (Figure 1.3b) allows it to absorb water from both sides of the surrounding soil (i.e., above and below). The unique design allows the wicking fiber to generate a higher capillary force. Thus, water from the adjacent soil is absorbed into the wicking fibers and can be easily transported along the deep grooved channels. Because the relative humidity of the air is usually less than 90% under most conditions, the suction caused by air at the surface of a pore is very high (>14MPa (>2 ksi)). If the end of the wicking geotextile is exposed to the atmosphere, there is a high suction gradient in the wicking geotextile from its buried end in the soil to the exposed end. The suction gradient is the driving force that continuously transports water from the buried end of the wicking geotextile yarns to the exposed end and water will be vaporized into the surrounding atmosphere at the exposed end. Theoretically, this process continues until the suction of the soil adjacent to the wicking geotextile is equal to the suction in the air. If time is long enough, all soils inside the pavement will be air-dried. Studies have shown that the wicking geotextile can effectively reduce the water content of adjacent soil corresponding to a suction value of 254 kPa (Lin et al. 2018b). At this point, even when repeated traffic load is applied on the pavement under undrained condition, the increase in pore water pressure will not be sufficient to build high positive pore water pressure and induce pumping.

There are several successful applications of using the wicking geotextile for different purposes. Zhang and Presler (2012) first used the wicking geotextile to prevent frost heave and thaw

weakening at Beaver Slide of the Dalton Highway. In 2011, the Alaska Department of Transportation and Public Facility used the wicking geotextile in Dalton Highway MP 197-209 Rehabilitation Project to improve a problematic soft ground. Five years of monitoring the test section proved very successful performance improvements were attained by utilizing the wicking geotextile (Currey 2016). Another successful example was the Parks Highway Broad Pass Railroad Overcrossing at the Milepost 196 in which wicking geotextile was used to treat a moisture-sensitive borrow that was exacerbated by the anomalously heavy and frequent rainfall in summer 2016. The treatment corrected the borrow workability problem and was considered an overwhelming success by the project team (Currey 2016).

The long-term performance and the potential clogging problem of the wicking geotextile have also been studied. Based upon scanning electron microscope (SEM) of 60 field samples obtained from the Beaver Slide and Coldfoot test section, Lin et al. (2016) concluded that clogging was not an issue in drainage function of the wicking geotextile. This study aims to extend the wicking geotextile application in mitigating pumping in the pavement.

1.4 Organization

This project objective is to study the efficiency of installing wicking geotextile under road shoulder to mitigate pavement pumping issue in Missouri. This report covers the construction of the test site on I-44 Highway in Philipsburg, Missouri in Chapter 2. In Chapter 3, preliminary interpretations of collected data from sensors are presented. Chapters 4 and 5 explain laboratory studies performed along with the field investigation to better understand the effect of wicking geotextile on pavement drainage. Chapter 6 covers the conclusions of this report.

CHAPTER 2: TEST DESIGN AND CONSTRUCTION PROCESS

2.1 Design

The aim of this project was to evaluate the efficiency of the proposed wicking geotextile in mitigating water pumping issues found along joints between the road surface and shoulder. Shoulder section 1F on Interstate 44 was used to study the proposed system. The testing site is located on the eastbound I-44 highway between the mile markers 117.2 and 117.4 with an approximate longitude and latitude of 37.551983° and -92.801741° , respectively. Figure 2.1 shows the aerial photo of the test site.

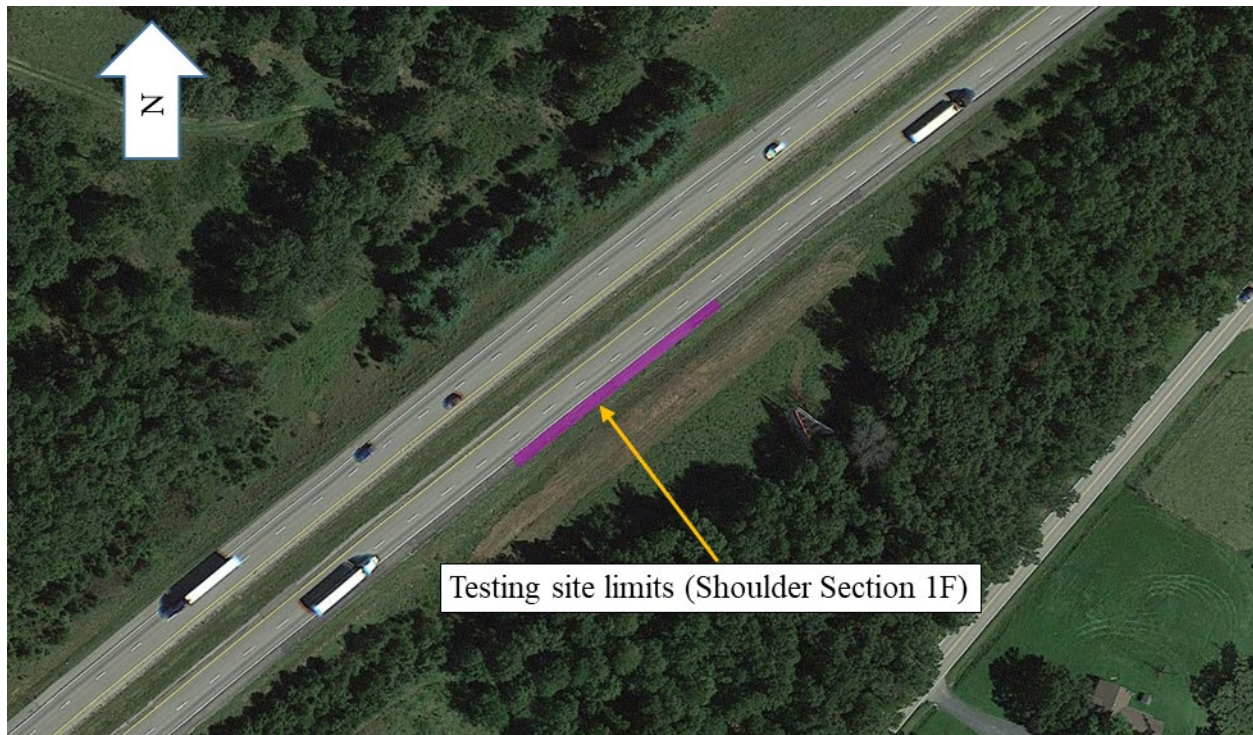


Figure 2.1 Aerial photo of the proposed testing site

Figure 2.2 shows the schematic plot of the test site design. The test site is 225 feet long. In order to study the effect of different placement methods on the drainage performance of wicking geotextile, the test site was divided into 3 sections as shown in Figure 2.2. From east to west, the three test sections were labeled as Control, Section 1, and Section 2 with lengths of 30 feet, 20 feet, and 175 feet respectively. The east section was left untreated without installation of wicking geotextile. It served as a control section and will be compared with the other two sections to evaluate the performance of the wicking geotextile on mitigating pumping. Section 1 was in the middle with installation of an L-shaped wicking geotextile. The red dotted line as shown in Figure 2.2 schematically shows the location of the installed wicking geotextile. As shown in Figure 2.2, the wicking geotextile was placed horizontally at the interface of the subgrade and base course layer with a depth approximately 18 in. below the road surface. At the interface between the driving lane and shoulder (inner edge of the shoulder), the wicking geotextile was folded up vertically to a height of approximately 12 in. This decision was made since the

pumping issue is mostly seen along the vertical interface of the driving lane and shoulder (inner edge of the shoulder) and cracks and potholes appear often in this region. Extending the geotextile to the location where damages are most likely to occur may facilitate the water drainage and have a beneficial effect on reducing the pumping issue over a longer period. Section 2 was at the west part of the test site and the wicking geotextile was placed horizontally at the interface of the subgrade and the base course layer with a depth approximately 18 in. below the road surface.

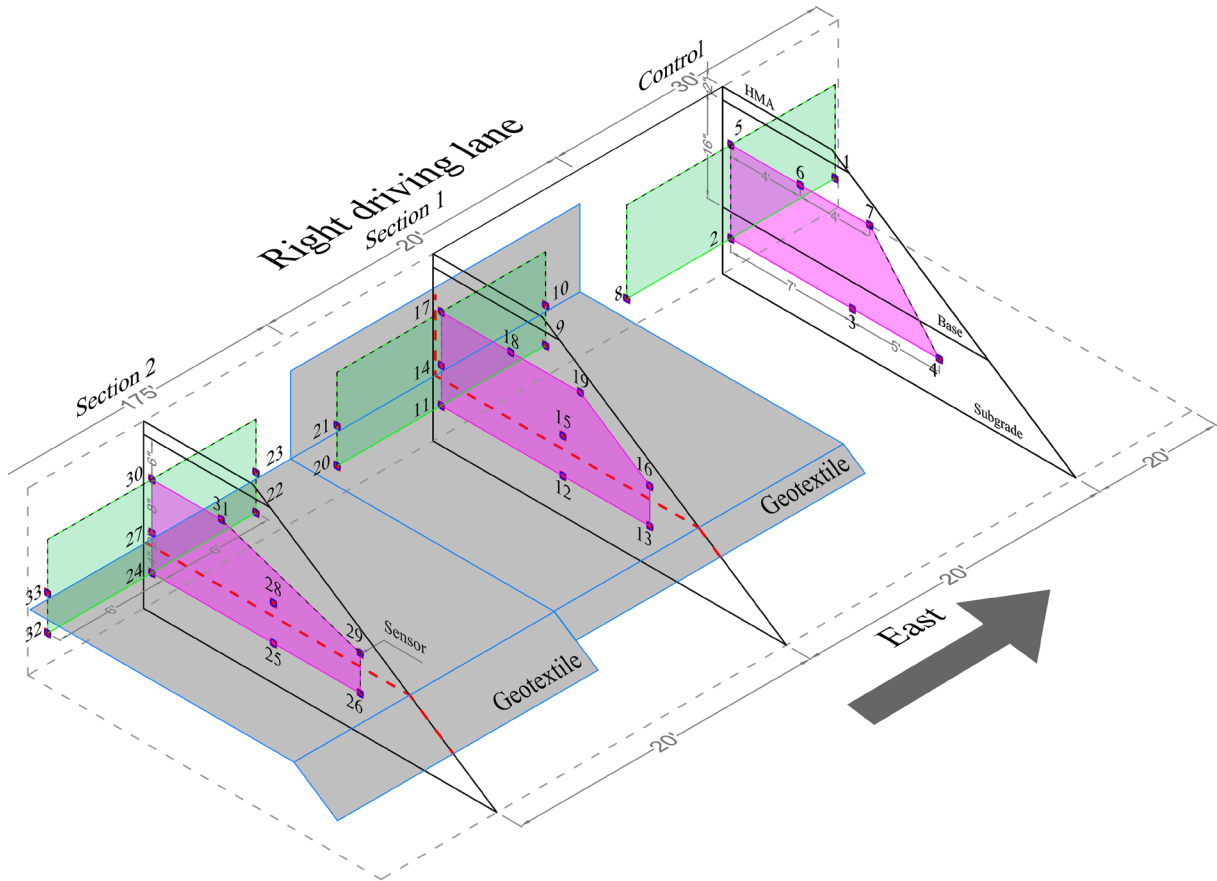


Figure 2.2 Schematic plot of test section design

In order to evaluate the performance of different treatments, a total of 33 moisture sensors with temperature measurements were installed at different locations of the three test sections as represented by the red solid dots in Figure 2.2. As shown in Figure 2.2, 6 sensors (labeled as 2, 3, 4, 5, 6, and 7) were installed in a cross-section in the control section along the transverse direction of the road, which was 20 feet away from the east end of the test site. The sensors were installed at two different elevations, one was 8 in. below the designed road surface (sensors 5, 6, and 7) in the base course materials, and the other (sensors 2, 3, and 4) was about 2-4 in. into the subgrade and 22 in. below the designed road surface.

In addition, two other sensors (labeled as 1 and 8 in Figure 2.2) were installed in the control section along the vertical interface of the driving lane and shoulder, which were at the same elevation of sensors 2, 3, and 4, and 6 feet away from sensor 2 on both sides.

Sensor installations in sections 1 and 2 were similar to that in the control section, except that an additional layer of 5 sensors was installed 2 in. above the wicking geotextile. Specifically, in section 1, sensors 10, 14, 15, 16, and 21 were installed directly above the sensors at the lowest elevation of 9, 11, 12, 13, and 20, respectively. The middle layer of sensors was roughly 16 in. below the designed road surface. In section 2, the additional layer of sensors were 23, 27, 28, 29, and 33. The purpose of this installation was to more closely monitor the moisture migration near the wicking geotextile. Please see Figure 2.2 for the detailed layout of the sensors.

2.2 Sensor Specifications

The 33 sensors used in this project were the “CS650 Water Content Reflectometer” sensors from Campbell Scientific® as shown in Figure 2.3 . These sensors have a rod length of 300 mm (11.8 in.) and probe head dimensions of 85×63×18 mm (83.35×2.48×0.71 in.), and can measure volumetric water content and temperature of the soil. The volumetric water content measurement range is 0% to 100% ±3% and the temperature measurement range is -50 to +70 °C ±0.5 °C (-58 to +158 °F ±0.9 °F).

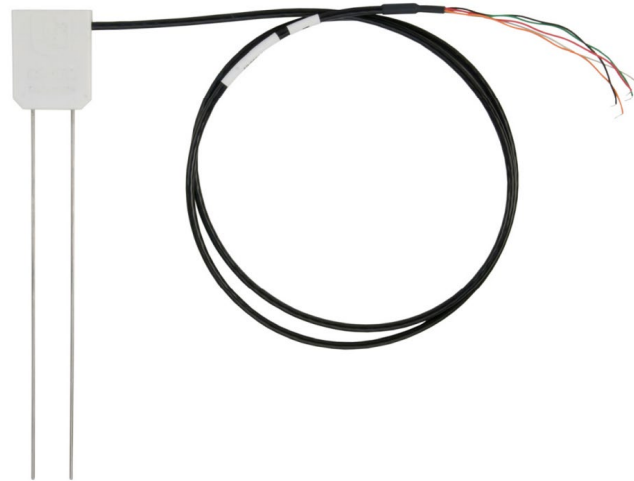


Figure 2.3 CS650 Water Content Reflectometer

2.3 Construction of Test Sections

Construction of the test sections started on Tuesday, September 25, and lasted 3 days to Thursday, September 27, 2018. Figure 2.4 shows the view of the site before construction. Since I-44 is an important Interstate Highway and generally has high traffic volume, all construction work must be taken place during the night when traffic volume was lower. During the day, only off-shoulder work was performed. On the first day, the locations of the 3 sections were marked. Some preparation work was also performed for sensor installation which included digging a trench for burying cables away from the road shoulder, and building a post for data logger and the solar panel installation (please see Figure 2.5).



Figure 2.4 View of the site before construction

This work continued during the afternoon of September 26, 2018. During the following night, the contractor started the first phase of construction on the shoulder. The existing asphalt layer was removed and the road shoulder was excavated to a depth of 18 in. where subgrade soils were found as shown in Figure 2.6. The subgrade soils were found to be high plasticity clay with red color.

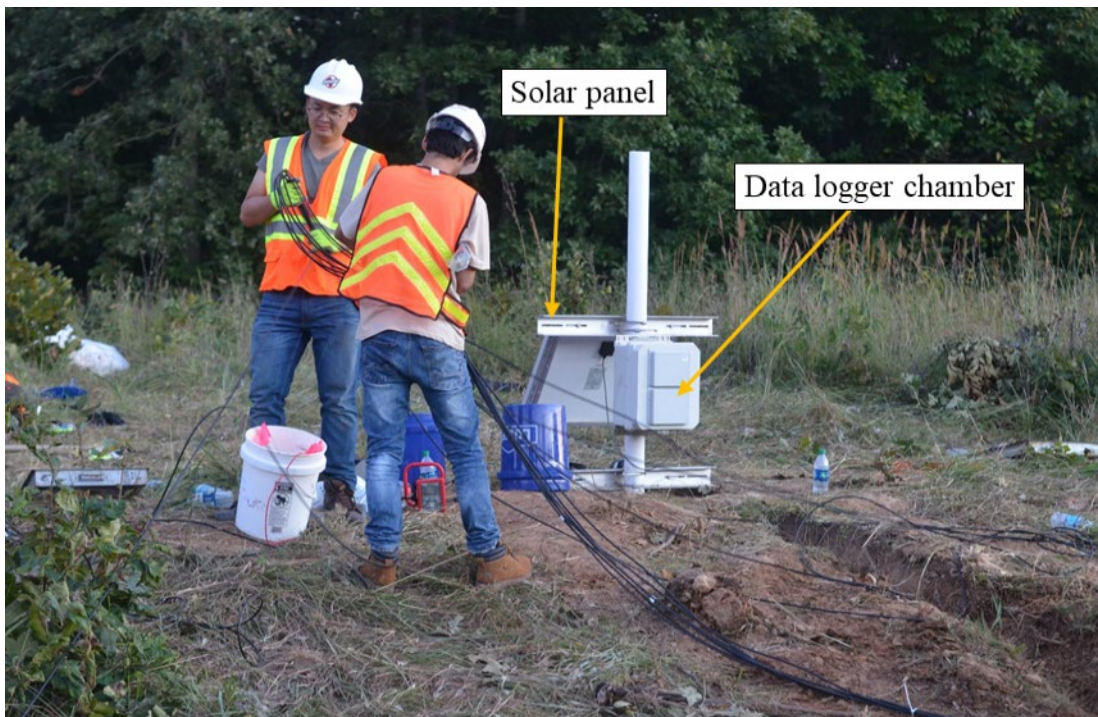


Figure 2.5 Off-shoulder work



Figure 2.6 View of the shoulder after excavation

The sensors were installed to monitor water content changes within the road shoulder in order to evaluate the performance of the wicking geotextile. Since the subgrade soils and the base course have different water storage capacity, the moisture contents in the two types of soils will be significantly different. More specifically, clayey subgrade soils can hold more water than the granular base course material. During rainfall events, water will migrate from base course soils, which have low moisture content, to subgrade soils, which has higher moisture content. In other words, water content is not the controlling factor for water to flow. Instead, water flows due to hydraulic head difference. In order to avoid the difficulties in future data analysis, it was decided that all sensors should be surrounded in the same type of soils during installation. In this way, we do not have to deal with the different water storage capacity associated with different soil types. For the same soils, water will flow from a location with high moisture content to another location with low moisture content if the elevation head is the same. In order to do so, in this study, the base course materials were firstly sieved using a 3/8 in. sieve and the soils passing the 3/8 in. sieve were used for sensor installation. For example, in order to install a moisture sensor in the subgrade soils as shown in Figure 2.7, a small hole was first made in the subgrade to a depth of 2-4 in. Then the hole was backfilled using the base course soils passing the 3/8 in. sieve. After that, the sensor was installed with its probes being horizontally placed in the fine base course soils.



Figure 2.7 Sensor installation in the subgrade soil

After the first layer of sensors were placed in the subgrade, the wicking geotextile was placed on top of the subgrade. Figure 2.8 shows the placement of the wicking geotextile in section 1. As mentioned previously, in section 1, the wicking geotextile was placed into a toppled L-shape by folding the wicking geotextile vertically along the edge of the driving lane as shown in Figure 2.8.

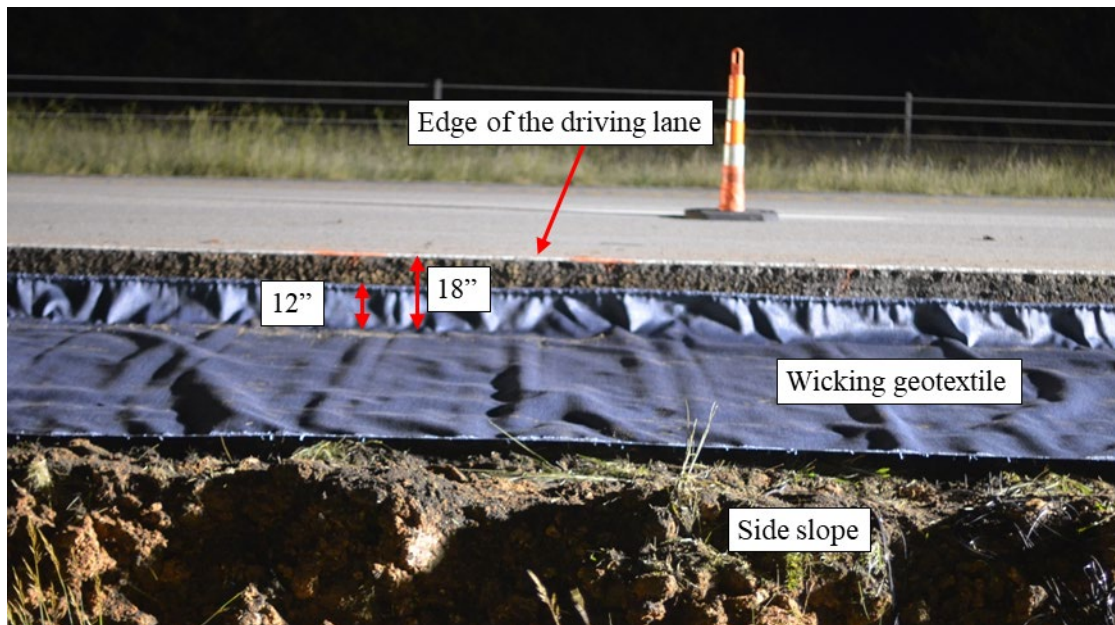


Figure 2.8 L-shaped placement of wicking geotextile in section 1

Figure 2.9 shows how the wicking geotextile was placed in section 2. As can be seen in Figure 2.9, the wicking geotextile in section 2 was placed horizontally directly on top of the subgrade layer, starting from the edge of the driving lane to the other side which was on the side slope of

the shoulder. Between sections 1 and 2, an overlap of 12 in. was made to ensure that the subgrade was fully covered by the wicking geotextile.



Figure 2.9 Horizontal placement of wicking geotextile in test section 2

Figure 2.10 shows how the sensors were installed above the wicking geotextile in section 2. The sensors were installed at approximately 2 in. above the geotextile in section 2. As discussed earlier, the sensors were installed in the sieved base course soils passing the 3/8 in. sieve. It would ensure the readings from all sensors were consistent within each other since the same soils were used. The finer base course soils also helped protect the sensors from being damaged by coarse aggregates during construction. The same procedures were adopted when sensors were installed above the wicking geotextile in section 1.

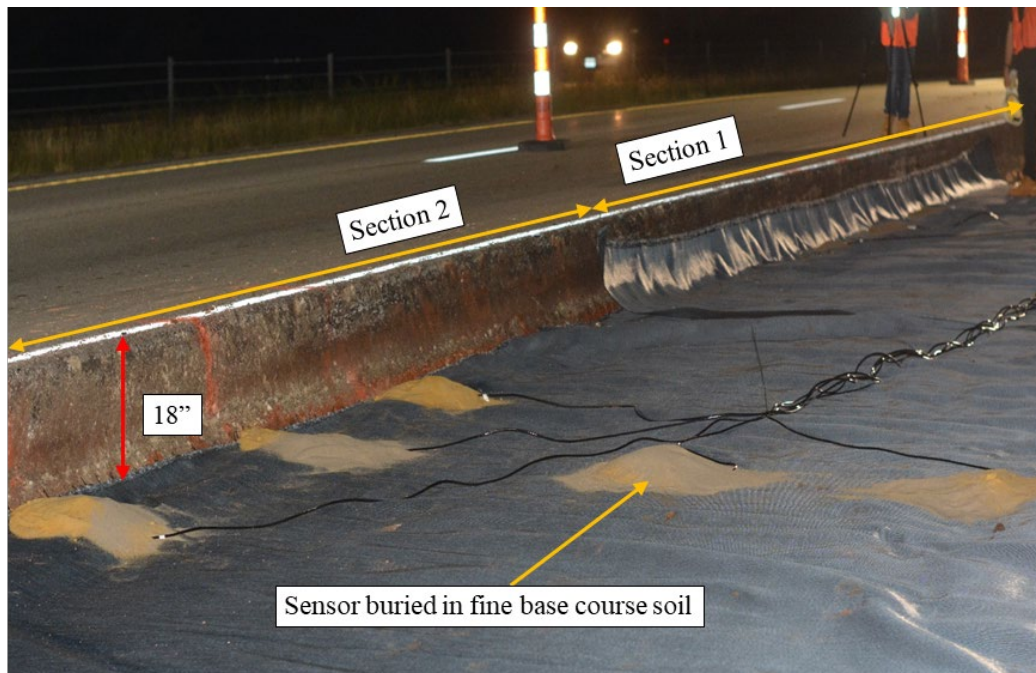


Figure 2.10 Sensor installation above the wicking geotextile in test section 2

After the second layer of sensors was installed, base course materials were directly dumped on the wicking geotextile and sensors and compacted to the designated elevation, which was the same as the existing road surface. Based on visual observation, the base course soil type was GP (Poorly graded gravel in the Unified soil classification system) with cobbles and occasional boulders. This backfill was then compacted using dynamic steel wheel rollers as shown in Figure 2.11.



Figure 2.11 Compaction of the base course

After the compaction was completed, on September 27, 2019, as shown in Figure 2.12 a trench-digger was used to dig trenches in the compacted base course soils the installation of the remaining sensors on the top layer as shown in Figure 2.2. The trench was dug to a depth of about 8 in. below the road surface. The remaining sensors were also installed in the sieved base course soils passing the 3/8 in. sieve, similar to previously installed sensors. After that, all the sensors were connected to the data logger and all cables were buried underground in order to protect them from being damaged. All the installation work completed on September 27, 2018.

After all the 33 sensors were installed, the contractor came back and excavated approximately 2 in. of the base course layer. Then the excavated base course layer was leveled and compacted. After that, asphalt materials were brought in and compacted to the elevation of the existing driving lane. Figure 2.13 shows the completed road shoulder. The photo was taken on October 5, 2018, during a revisit to the test site. It was noticed that the edge of the wicking geotextile was exposed to the atmosphere as designed.



Figure 2.12 Preparing a trench for sensor installation using a trench-digger

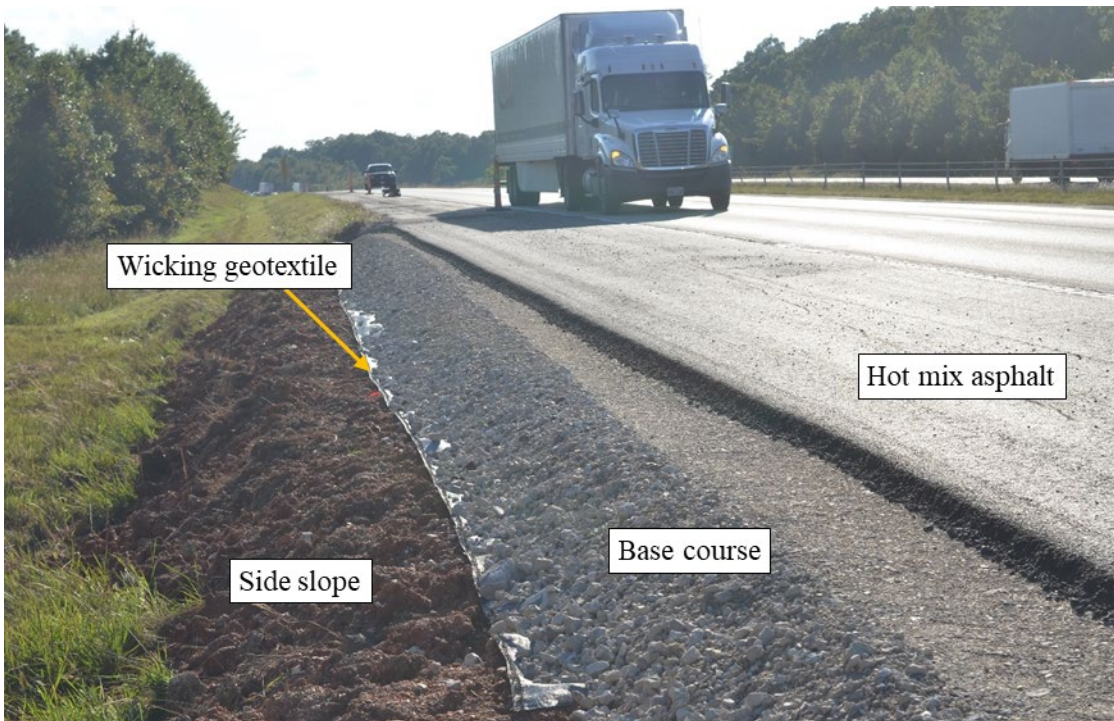


Figure 2.13 View of the test site after construction

In order to acquire preliminary results, the data logger readings were transferred to a portable computer. It was found that one of the sensors (sensor 13) was not transmitting data due to a connection problem. Although the connection was restored that day, the first week's data was not available for this sensor. Figure 2.14 shows the location of the designed sections after the construction was finished.

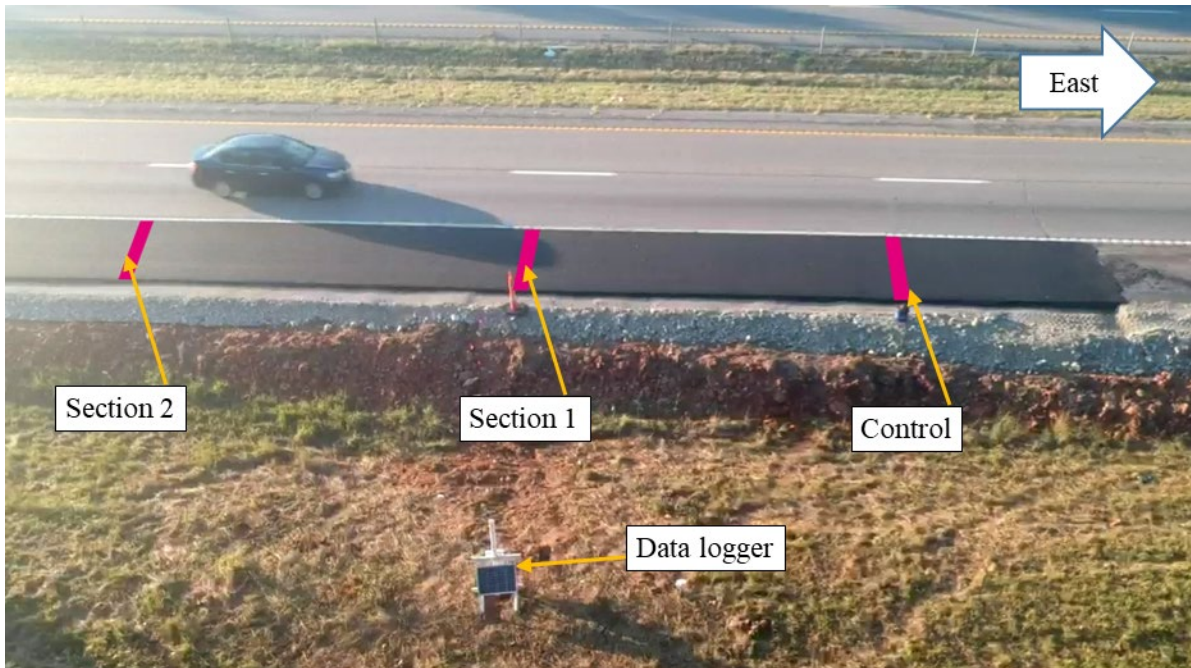


Figure 2.14 Location of the test sections after paving the road shoulder

On November 18, 2018, another visit was made to the site in order to collect data. It was found that the unpaved part of the shoulder was graded. This work made the unpaved shoulder have a uniform slope, but the edge of the wicking geotextile was completely covered by base course soils. Figure 2.15 shows the final configuration of the test site.

As previously mentioned, the drainage performance of the wicking geotextile could be improved by exposing the end of the wicking geotextile to the atmosphere. Thus, on February 9, 2019, about 1 foot of the edge of the wicking geotextile on the side slope was exposed along sections 1 and 2 by removing the base course as illustrated in Figure 2.16 .



Figure 2.15 The final configuration of the test site



Figure 2.16 Exposing the outer end of the wicking geotextile on February 9, 2019

2.4 3D Reconstruction of the Test Site

A number of laser scanings were performed to reconstruct the 3D geometry of the test site situation during different stages of the construction of the test site. For this purpose, Leica ScanStation P40 was used. This can be helpful to quickly get a 3D geometry of the test site which may be used in further analyses. Figure 2.17 through Figure 2.20 shows the reconstructed 3D geometry of the test site at different stages of construction. The 3D geometry can be used for future more comprehensive studies.

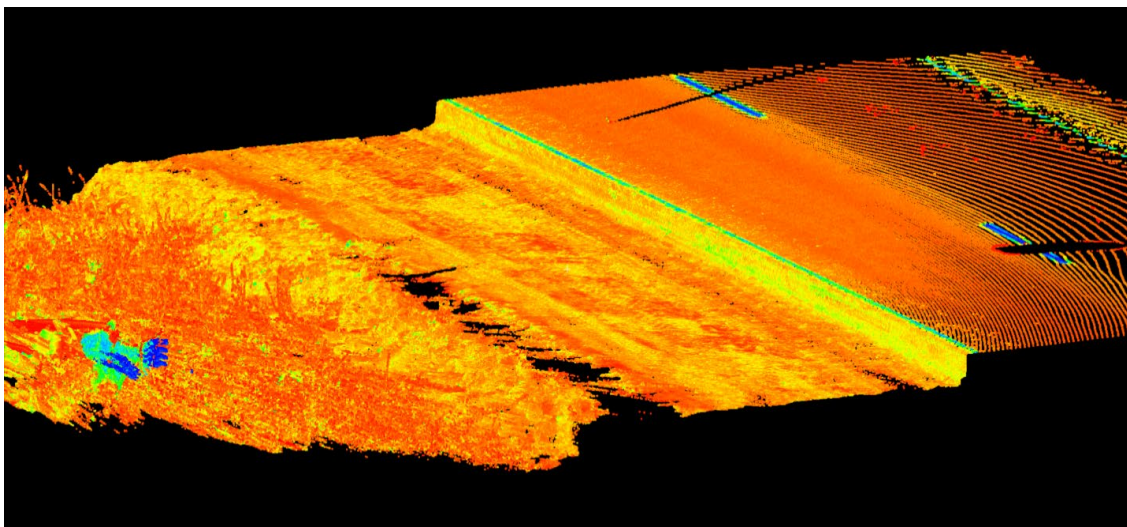


Figure 2.17 Scan data after excavation to the depth of 18in.

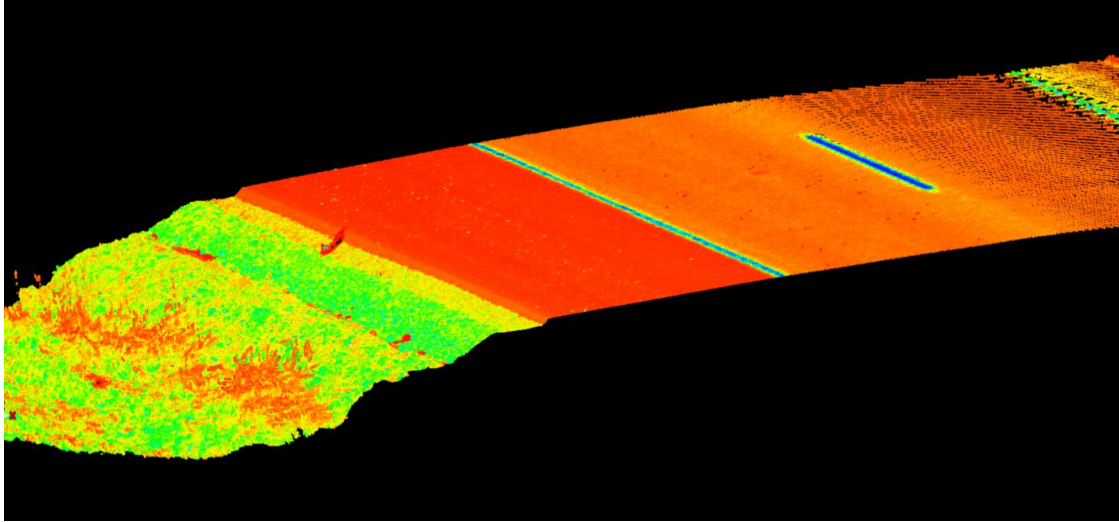


Figure 2.18 Scan data after paving the shoulder

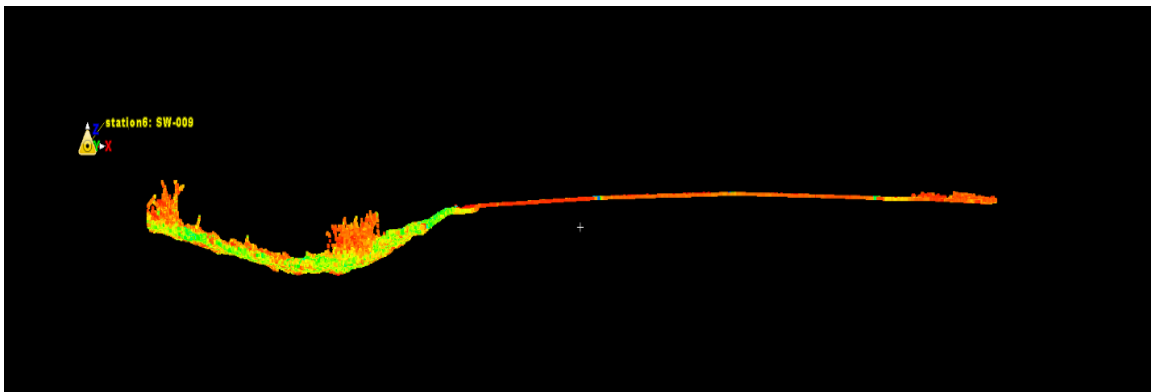


Figure 2.19 The final constructed cross-section

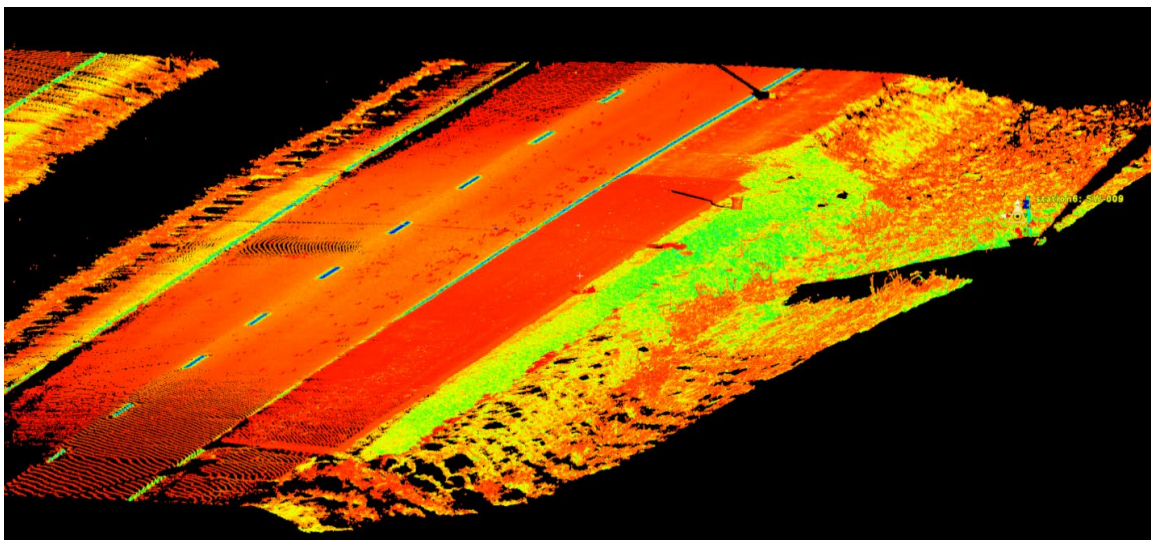


Figure 2.20 Site overview after construction

CHAPTER 3: PRELIMINARY RESULTS

3.1 Introduction

This chapter discusses the results obtained from the field test site during one year after its construction. First, the climatic conditions of the test site will be detailed. Then, the variation of volumetric water content (VWC) at different sections of the test site will be discussed. Finally, the spatial VWC contour plots of the test sections will be analyzed at which the performance of the wicking geotextile in reducing water content was evaluated.

3.2 Local Climatic Conditions

The moisture content in the pavement structure is closely related to local climatic conditions. Hence, it is important to acquire local climatic data and compare it with the changes in moisture content in the pavement when analyzing the field monitoring results. Figure 3.1 shows the relative locations of two of the closest weather stations on each side of the test site (Camdenton and Vernon). In this study, the climatic data from the weather station which was the closest to the test site was chosen to represent the climatic conditions at the test site. The weather station closest to the test site was located 30 miles north, at Camdenton, Missouri.

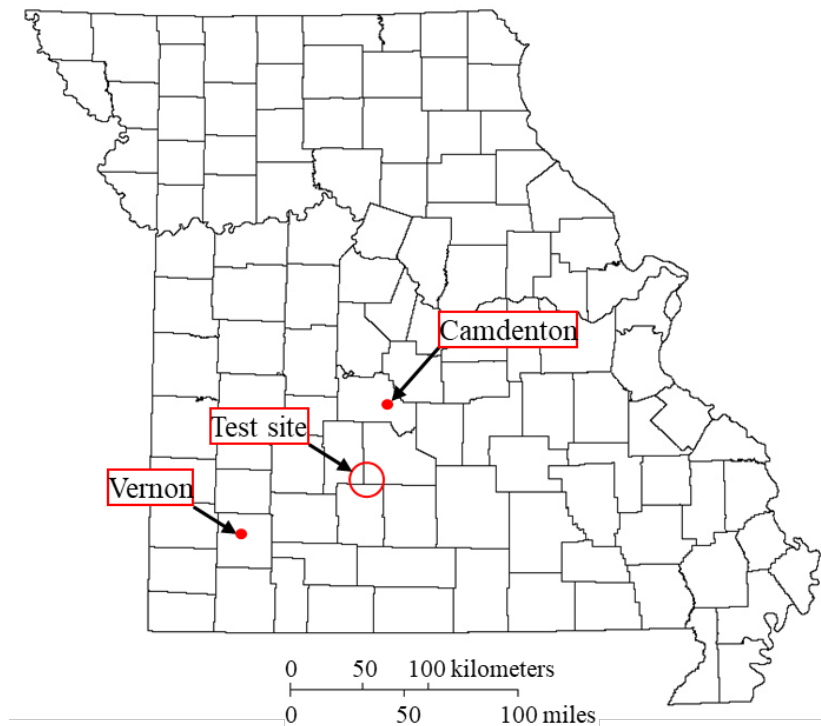


Figure 3.1 Relative locations of two closest weather stations to the test site

Figure 3.2 shows the climatic data obtained from Camdenton weather station during the monitoring period from September 28, 2018, to October 3, 2019. Figures 3.2a-3.2e show the daily total solar radiation, mean wind speed, mean air temperature, relative humidity of air, and precipitation at Camdenton weather station respectively. Precipitation is related to the amount of

water that is available for infiltration into the pavement system. As shown in Figure 3.2e, precipitation was observed in 115 days out of 378 days, with an accumulative value of 934 mm (36.8 in.). Most of the precipitation happened from December 2018 to August 2019. The amount of precipitation was significantly less in October through December 2018 and after August 2019.

The potential evapotranspiration represents the maximum ability of a certain climatic condition to vaporize water and is a function of solar radiation, wind speed, air temperature, relative humidity, and other factors. Although the actual evapotranspiration could be significantly different from the potential evapotranspiration due to the availability of water in the pavement system and other factors, the potential evapotranspiration is a good indication of the amount of water that could be lost from the pavement. The daily potential evapotranspiration was calculated based on ASCE's standardized reference evapotranspiration equation (Walter et al. 2000), which is also shown in Figure 3.2e.

Different from precipitation, evapotranspiration happened every day during the monitoring period. The reason for this is due to the fact that the relative humidity in the air was always less than 100% as shown in Figure 3.2d. As shown in Figure 3.2d, the relative humidity was normally between 50-90% for a majority of the period. This resulted in a high suction value in the air. During the whole monitoring period, there was only one day (February 11, 2019) in which the relative humidity was 100%, which lasted for only 2 hours.

The calculated cumulative potential evapotranspiration in the same analysis period was 1022 mm (40.2 in.), which was nearly 10% more than the total precipitation. It is worth noting that the differences between the actual water infiltration and water loss through evaporation could be significantly larger than 10%. This is attributed to the fact that a rainfall event often lasted only for a few hours with much higher intensities than daily precipitation. As a result, a large portion of the rainfall ran off during rainfall events and did not infiltrate into the ground.

Also, based on the air relative humidity and mean temperature, the air suction was calculated as shown in Figure 3.2f. The calculated air suction was always greater than 1 MPa (145 psi), and generally between 30-180 MPa (4350-26100 psi). Under such levels of suction, the soils on the slope of the road can be completely air-dried. Once the surface soils are air-dried, the water phase in the soils become discontinuous, which results in extremely low unsaturated permeability. It is therefore very difficult for water inside the pavement to come out even though the huge suction difference still exists between the soil inside and the surrounding atmosphere. However, as it is discussed before, with the help of multiple microchannels in the wicking geotextile, water can be easily transported from inside to the edge of the road shoulder and vaporized into the atmosphere. This suction is the driving force that drags the excess water out of the pavement through the channels in the wicking fibers as shown in Figure 1.3. This is the working mechanism of the wicking geotextile.

As mentioned in chapter 2, the wicking geotextile was completely buried in the soils when the test sections were completed. In order to study the effect of air exposure of the wicking geotextile on the moisture content changes in the pavement, the research team removed some soils at the outer edge of the wicking geotextile in sections 1 and 2 on February 9, 2019, to expose approximately one foot of wicking geotextile to the air. To facilitate future comparison,

green dotted vertical lines were added to Figure 3.2 and the following figures on February 9, 2019.

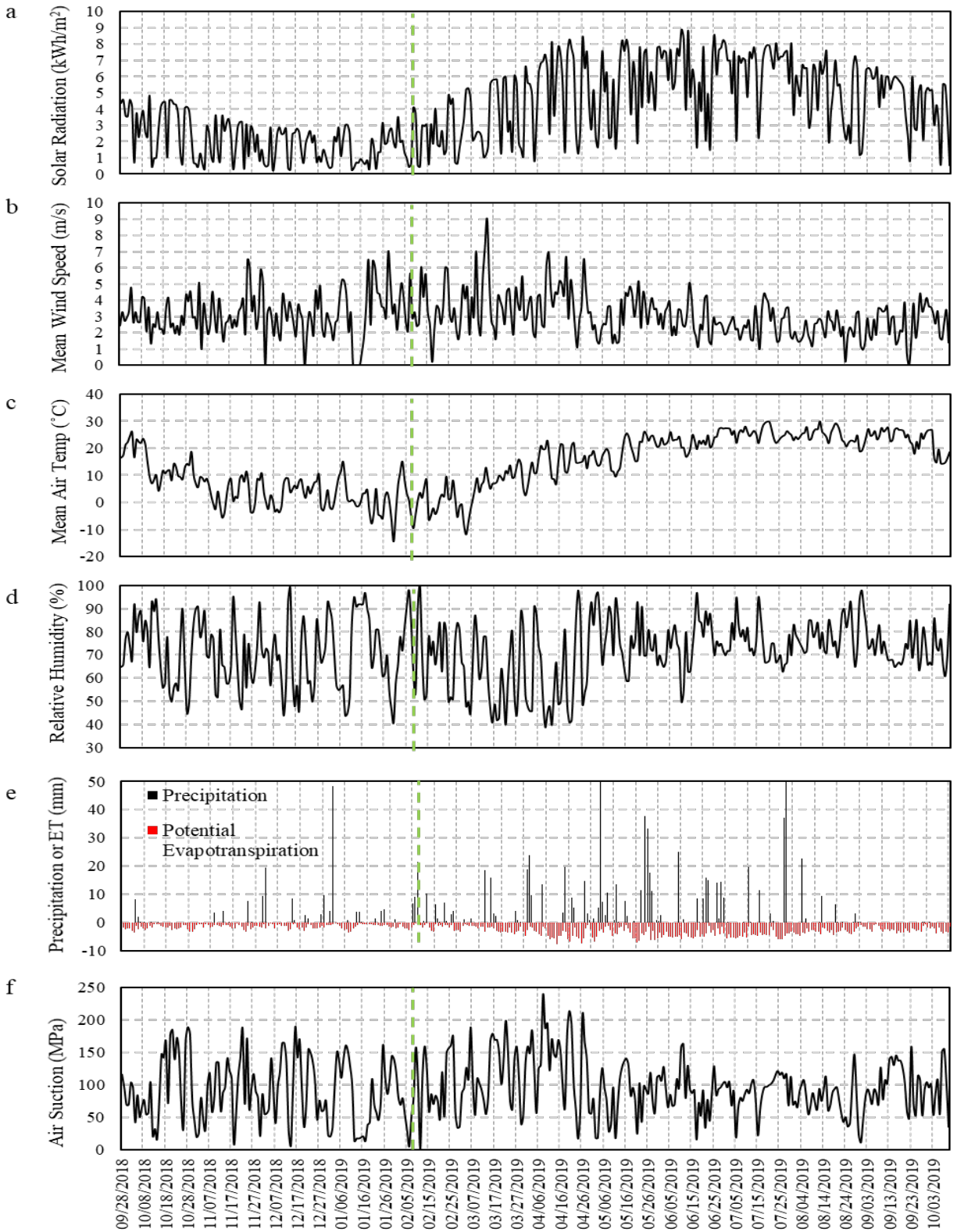


Figure 3.2 General climatic information based on data obtained from a weather station at Camdenton, Missouri. a) Total solar radiation, b) Mean wind speed, c) Mean air temperature, d) Relative humidity, e) Precipitation and potential evapotranspiration, f) Air suction.

3.3 Volumetric Water Content at Different Sections

This section discusses the variations of the VWC at individual sensor locations in the three test sections. As mentioned before, one of the sensors (sensor 13) did not record any data for one week prior to the first visit to the site after the construction was finished. After that, the problem was resolved and the sensor was restored to operational mode.

Figure 3.3 shows the volumetric water content (VWC) readings from sensors 4, 13, and 26, which are at the outer edge of the subgrade in the control section, section 1, and section 2 respectively (please refer to Figure 2.2). As can be seen in Figure 3.3, all the initial VWC readings were low, ranging from 19% to 28% with an averaged value of 23%.

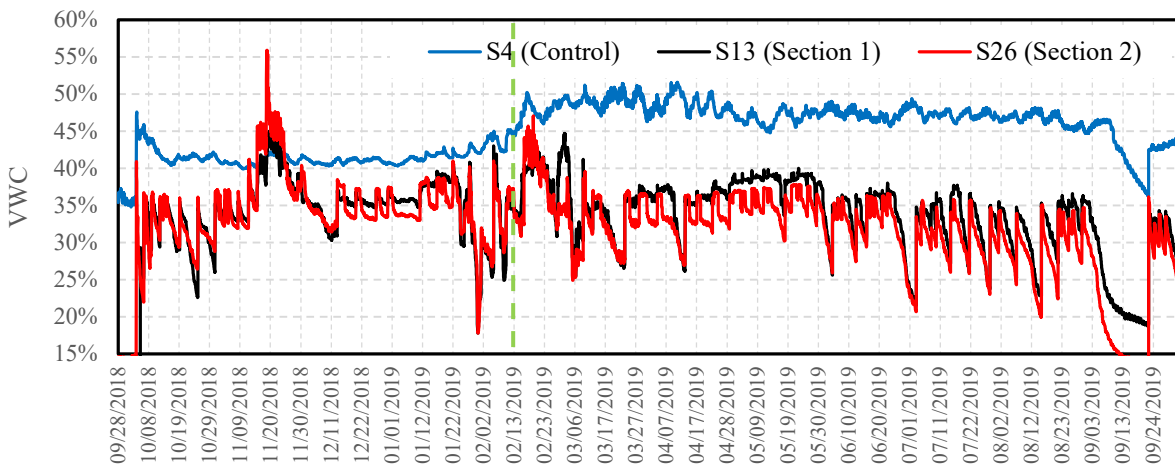


Figure 3.3 VWC at the outer edge of the subgrade

However, after the first rainfall on October 5, 2018, moisture contents at all three test sections of the pavement increased significantly. It can be seen in Figure 3.3 that VWC in the control section decreased to above 40% after the first rainfall was over, but never returned to the initial VWC which was observed right after construction of the test section. This implies that the performance of the pavement was always lower than that immediately after the construction due to rainfall infiltration. The VWC in winter 2018 was around 40%. However, in the spring of 2019, due to more frequent rainfall events, it increased to the range of 45-50%.

As shown in Figure 3.3, there were many sudden increases in VWC in the test sections. A reasonable assumption would be that these peaks were caused by rainfall events as shown in Figure 3.2e. Careful comparison between Figures 3.2e and 3.3, however, indicated that not all of the VWC peaks matched with the rainfall data. In fact, there were some peaks in the VWC in Figure 3.3 without any corresponding precipitation in Figure 3.2e. For example, on October 25, 2018, there was a VWC peak in Figure 3.3, but no rainfall event as indicated by Figure 3.2e. This might be attributed to the fact that some rainfall events only occurred in the small local

region of the test site but did not cover the location of the weather station where the climatic data was collected. This assumption was verified by investigating the second closest weather station (Vernon weather station) to the field section location. Climatic data obtained from Vernon weather station showed that the peak on October 25, 2018, in the graph of Figure 3.3 only appeared in rainfall in this station. As shown in Figure 3.1, the Vernon weather station was located approximately 60 miles southwest of the test site. In general, almost all of the peaks in the WVC data were from either Camden or Vernon weather station, indicating the consistency in the moisture measurements.

Figure 3.3 also shows that the overall VWC in the control section except for a short time was much higher than those in sections 1 and 2. As can be seen, the fluctuation magnitude in VWC of the control section, which was 8%, was much less than those for sections 1 and 2, which was 15%. The reason for this is due to the better drainage performance of the improved sections. During a rainfall, VWC in sections 1 and 2 increased more and quickly decreased to a much lower value after rainfall stopped. However, in the control section, due to an overall worse drainage performance, water accumulated by the recurring rainfalls leading to increased VWC. Since water could not drain as fast as the improved sections, the control section showed less fluctuation amplitude during each rainfall. This indicates that the overall permeability of the system was relatively lower in the control section. The low permeability delayed the increase in the water content during each rainfall. In the same way, it prevented quick water loss from the soil after the rainfall.

It can also be seen from Figure 3.3 that the VWC in sections 1 and 2 during late November was much higher compared with that in the control section. The increase in VWCs in the two sections was the result of recurring heavy rainfalls. Water may have started to flow back into the pavement through the wicking geotextile. At this time, the soil deep inside the pavement was still under unsaturated condition, while the outside slope was saturated. As a result, water flowed back into the pavement. However, once rainfalls stopped and the runoff water dissipated, the outside atmosphere was drier and water started to drain out of the pavement. It is also worth noting that the effect of water backflow is not significant for at least three reasons. First, as it was discussed before, on average rainfalls occurred only 1 out of every 3 days. Secondly, each rainfall event only lasted a few hours. Thus, this would increase runoff water and decrease the actual amount of water permeating the pavement. Lastly, the hydraulic gradients for backflow during rainfall events were much smaller than those during a sunny day with drainage.

As mentioned previously, the soil used for the base course layer consisted of cobbles and occasional boulders. This potentially resulted in nonuniform void distribution inside the base course layer and varying bulk density in the base course layer. The moisture sensors used in this study measure the volumetric moisture content in the soils surrounding the sensor. The nonuniform void distributions made the measured VWC fluctuate and difficult to analyze. In order to better understand the monitoring results, the changes in VWC for each sensor relative to its initial readings were used to explain the test results instead of the absolute VWCs at different locations. Figures 3.4 and 3.5 show the changes in VWC at the inner edge of the shoulder section (vertical interface of the shoulder and the right driving lane) at the top of the base course and subgrade, respectively.

Figure 3.4 shows the changes in VWC at the inner edge of the base course at the shallowest sensor level in control section (sensor 5), section 1 (sensor 17) and section 2 (sensor 30) relative to their initial readings. It can be seen from Figure 3.4 that the relative VWC in section 2 was about 2-3% less than section 1 and control section until February 9, 2019, when the edge of the wicking geotextile was exposed to the atmosphere. It can also be seen that relative VWC in section 1 was occasionally slightly higher than the VWC in the control section before February 9, 2019. However, after the edge of the wicking geotextile in section 1 was exposed, VWC in section 1 started to deviate from the control section and section 1 started to perform better in terms of draining moisture out of the pavement. This is more obvious after March 2019. By the end of June in 2019, the VWC in section 1 and section 2 compared with the control section was approximately 5% and 10% lower, respectively.

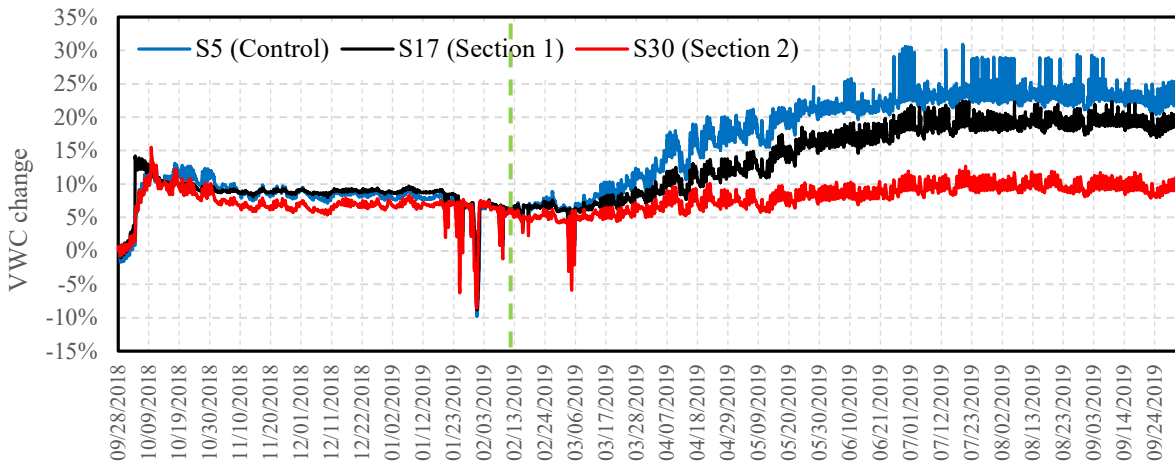


Figure 3.4 Relative VWC in different test sections at the top of the base course and the inner edge of the base course

It can also be seen from Figure 3.4 that from mid-January to early April 2019, there are a number of sudden drops in VWC of all of the sensors. By comparing Figures 3.2 c and 3.4, it is found that these drops are likely to be the result of soil freezing during this period. The drops on air temperatures matched well with the sudden drops in VWC during the same period. The moisture sensors used in this study measure the unfrozen volumetric moisture content only. When prolonged durations of subzero temperatures caused subgrade soils and moisture contained within to freeze, the unfrozen moisture content in the soils decreased significantly.

Figure 3.5 shows the relative VWC inside the subgrade in control section (sensor 2), section 1 (sensor 11), and section 2 (sensor 24) at the edge of the driving lane. It can be seen that relative VWCs in sections 1 and 2 increased significantly during each heavy rainfall, but only for a very short time.

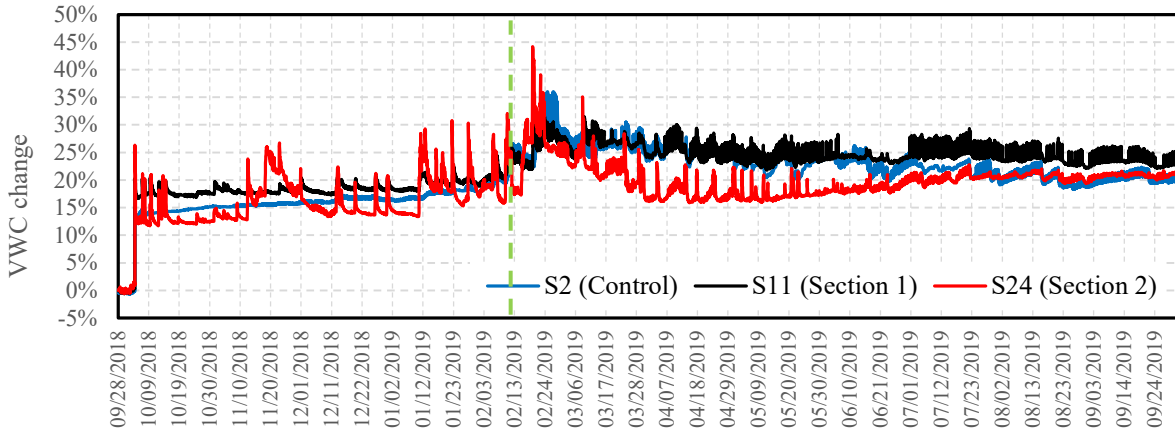


Figure 3.5 Relative VWC in the subgrade at the edge of the driving lane.

As explained before, this happened because the exposed edge of the wicking geotextile became saturated and water started to move into the pavement through the wicking geotextile. However, after the rainfall stopped and the exposed edge of the wicking geotextile started to dry, the wicking geotextile started to drain moisture out of the pavement and VWC decreased quickly. It can be seen that relative VWC in section 2 was up to 6% less than those in the control section and section 1 between two successive rainfall events. This is attributed to the fact that in section 2, the wicking geotextile had the most exposure to the atmosphere, which resulted in more water loss.

3.4 VWC at Different Elevations of Each Section

In the following sections, the results of VWC at different elevations of each test section are discussed.

3-4-1- Control section

Figure 3.6 shows the variations of VWC at sensors 2 and 5, which are at the inner edge of the control section, respectively. As shown in Figure 2.2, sensors 2 and 5 are located at 8 in. and 22 in. below the final road surface respectively. The initial VWC at sensor 5 is around 23% corresponding to the initial moisture content of the base course during placement and compaction. All volumetric water content readings showed a significant jump on October 4, 2018, during the first rainfall after the construction of the test sections. As shown in Figure 3.1a, it is obvious that there was a rainfall event on October 4 with a total daily precipitation of 0.33 in. (8.3 mm). After the first rainfall, the VWC in the base course (sensor 5) continuously decreased until March 2019. This might be attributed to less frequent rainfall, gravity drainage of infiltrated water, and soil freezing during this period. In contrast, the VWC at the subgrade (senor 2) increased gradually over the same period due to the accumulation of infiltrated water.

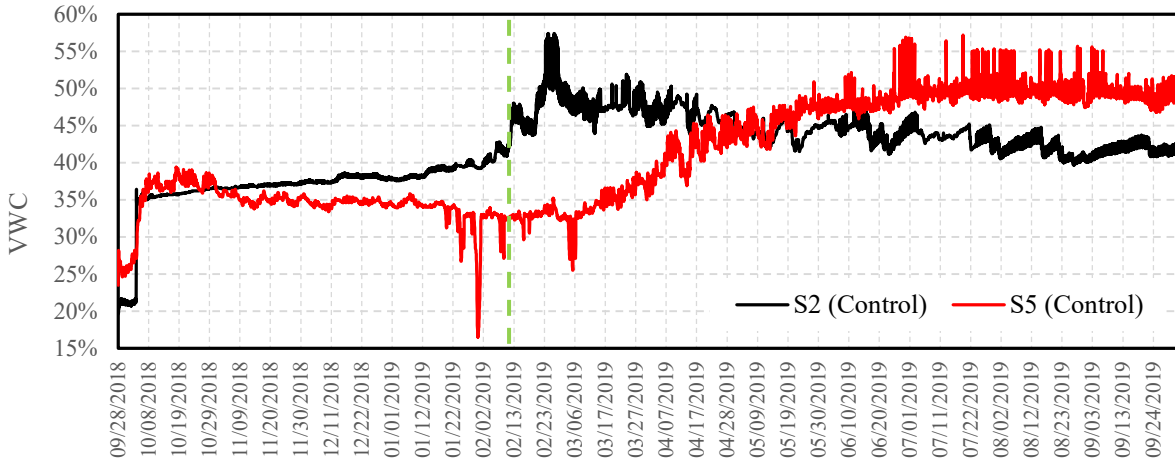


Figure 3.6 Variation of VWC in the control section at different elevations at the inner edge of the shoulder

In early 2019, the VWC at sensor 5 experienced a few sudden drops due to soil freezing. In contrast, soils at sensor 2 did not experience such sudden drops. This is likely due to the fact that sensor 2 was buried deeper into the pavement, the freezing front didn't reach to the depth of sensor 2. In fact, when sensor 5 was not experiencing sub-zero temperature, the VWC in sensor 5 kept increasing consistently. At this time, there were several rainfall events in a short time as shown in Figure 3.2e. The increase in the VWC of sensor 2 is believed to be the result of water infiltration from these rainfall events.

After the winter was over in March 2019, the VWC in the base course layer (sensor 5) increased gradually starting from 32% for a period of around 2 months. By the end of June 2019, the average VWC in the base course reached 50% and remained constant. In the meantime, the average VWC in the subgrade decreased from around 50% in March to 42% in October 2019. The results seemed strange since the soil at higher elevations should have lower moisture content. This might be attributed to non-uniform soil distribution in the test section. If the soils at the top have more fines or smaller void due to better compactions, these soils can hold more water compared with the soils at the bottom with less fines content or lower density.

Similarly, Figure 3.7 shows the variation of VWC in the middle of the control section in the transverse direction at sensor 3 (22 in. below road surface) and sensor 7 (8 in. below the road surface). The trend of VWC is similar to those observed in Figure 3.6 at the inner edge of the control section. The VWCs at sensor 3 were always higher than those at sensor 7. The results seemed reasonable.

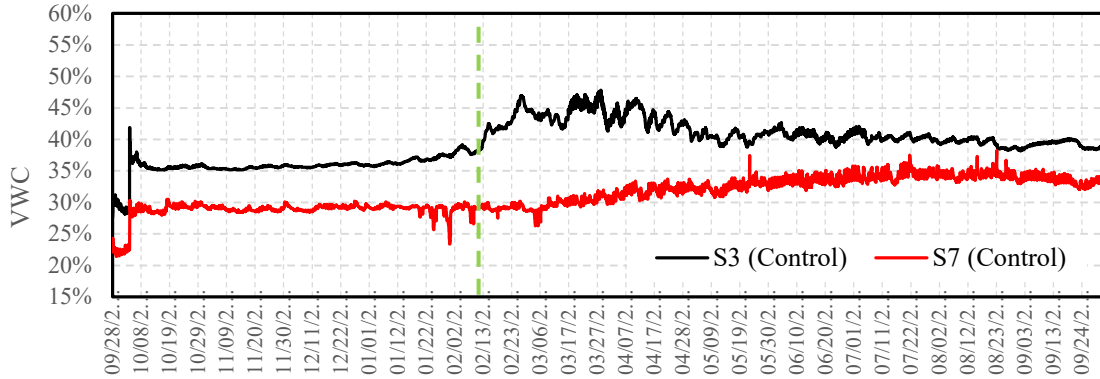


Figure 3.7 Variation of VWC in the control section at different elevations at the middle of the shoulder

3-4-2- Section 1

Figures 3.8 through 3.10 show the variations of the VWC at different locations of the road shoulder for sensors at different elevations of section 1. All volumetric water content readings showed a significant jump on October 4, 2018, during the first rainfall after the construction of the test sections. It is also found that after October 4, 2018, the VWCs at the bottom layer of sensors (located in subgrade) were higher than those at higher elevations (in the base course).

Figure 3.8 shows the variations of VWC at sensors 11, 14, and 17 in section 1 at the inner edge of the shoulder (from bottom to top as shown in Figure 2.2). As can be seen, prior to January 2019, except for some peaks due to rainfall, VWC at sensor 17 was similar to that in the subgrade (sensor 11) with a value of approximately 36%. However, from January to March 2019, the moisture content in sensor 17 reduced due to partial soil freezing. The sharp decrease in VWC readings in this period corresponds to the sudden freezing of the soils surrounding the sensor. On the other hand, the moisture content in sensor 11 generally increased with time if the peaks caused by the rainfall were not considered. The results were reasonable for two reasons. First, sensor 11 was located in the subgrade where the temperature was always higher than 0°C (32 °F). It means that the subgrade did not experience any freezing in winter. Secondly, the precipitation in early 2019 increased which increased the water infiltration into the pavement and results in an increase in moisture content. By June 2019, the VWC at different elevations of section 1 reached a constant value of approximately 45%. In general, VWC at sensor 14 located at the bottom of the base course layer was always between the VWC at sensor 11 and 17.

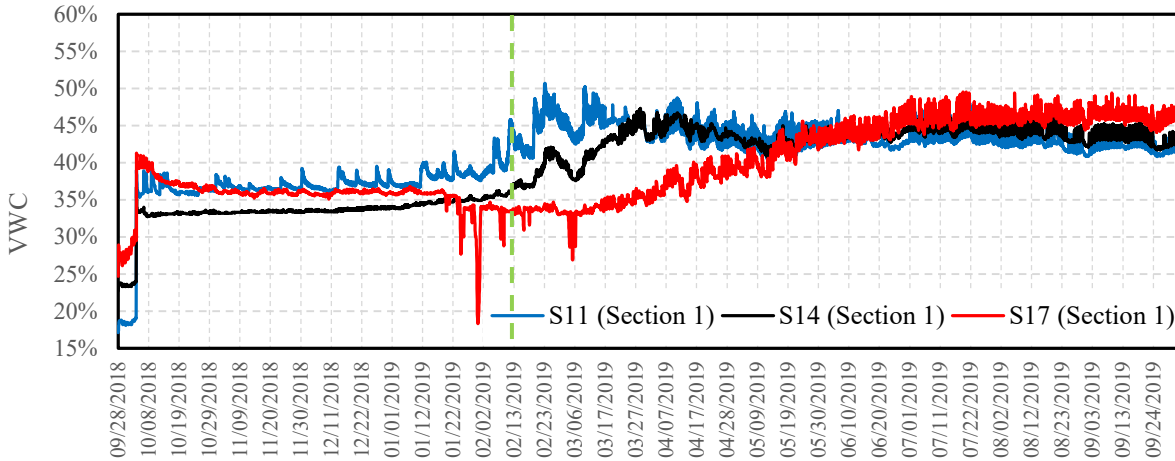


Figure 3.8 Variation of VWC in section 1 at different elevations at the inner edge of the shoulder

Figure 3.9 shows the variations of VWC at sensors 12, 15, and 19 in section 1 in the middle of the shoulder. VWC at sensor 12 (in the subgrade) was around 40% before February 2019. This value increased to 43% during the spring and summer of 2019 with increasing precipitation. The changes in VWC at sensors 19 and 15 were similar except that the VWC at sensor 19 had many peaks due to rainfall, which were not seen at sensor 15. The WVC values slightly increased from 33% in winter 2018 to 35% in spring and summer 2019 if the peaks caused by rainfall events were not considered.

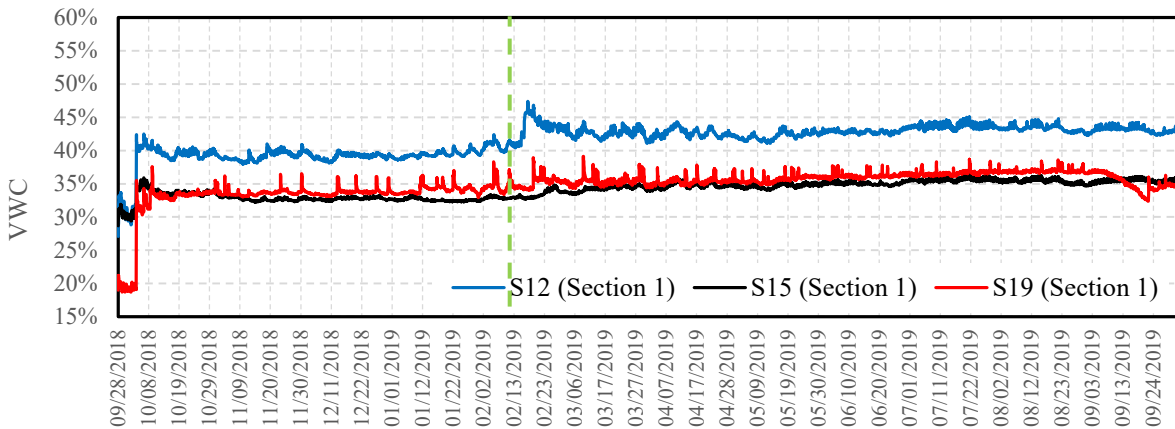


Figure 3.9 Variations of VWC at sensors 12, 15, and 19 in section 1 in the middle of the shoulder

By comparing the VWCs at sensors 14 and 17 in Figure 3.8 with VWCs at sensors 15 and 19 in Figure 3.9, respectively, it was found that VWCs in Figure 3.8 were generally higher than those in Figure 3.9, even if the corresponding sensors were at the same elevations. This implies that rainfall infiltration was not uniform across the whole road shoulder. Instead, water infiltrated along the interfaces between the old pavement and the newly constructed road shoulder and

migrated along the wicking geotextile. This might be the reason why the VWC at sensor 15 was much lower than those at sensor 14 after March 2019.

Figure 3.10 shows the variations of VWC at sensors 13 and 16, which is at the outer edge of section 1 during the monitoring period. In general, VWC at sensor 16 were 5%-8% lower than that at sensor 13 at the same time, although the trends of VWC changes were similar. This indicated that the base course layer on top of the wicking geotextile was much drier than the subgrade layer. However, during the heavy rainfalls on November 21, 2018, and February 19, 2019, the VWCs at the two sensors reached the same value.

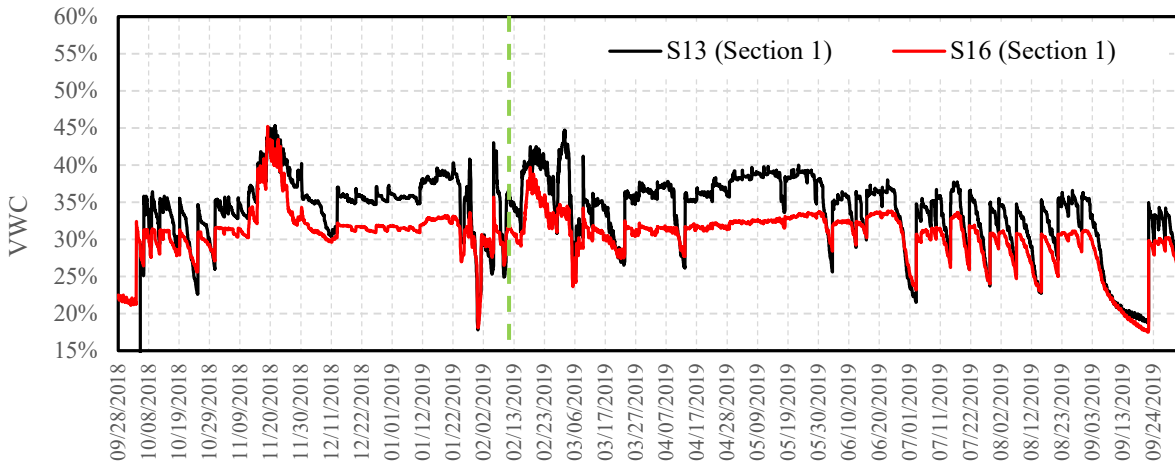


Figure 3.10 Variation of VWC in section 1 at different elevations at the outer edge of the shoulder

3-4-3- Section 2

Figure 3.11 through 3.13 shows the variations of the VWC at different locations of section 2 for sensors at different elevations. In general, the trends in the VWC changes are similar to those in Figure 3.8 through 3.10 in section 1, thus the explanations for them will not be repeated again. More detailed comparisons between the control section, section 1 and section 2 will be made when the VWC contour plots are presented in the later sections.

3.5 VWCs at the Critical Locations for Pumping

Pumping usually occurs at the interface between the driving lane and the shoulder. Thus, reducing the water content at these locations is crucial for pumping mitigation. The following paragraphs compare the VWC changes in sections 1 and 2 at the critical interface for pumping in the pavement structure.

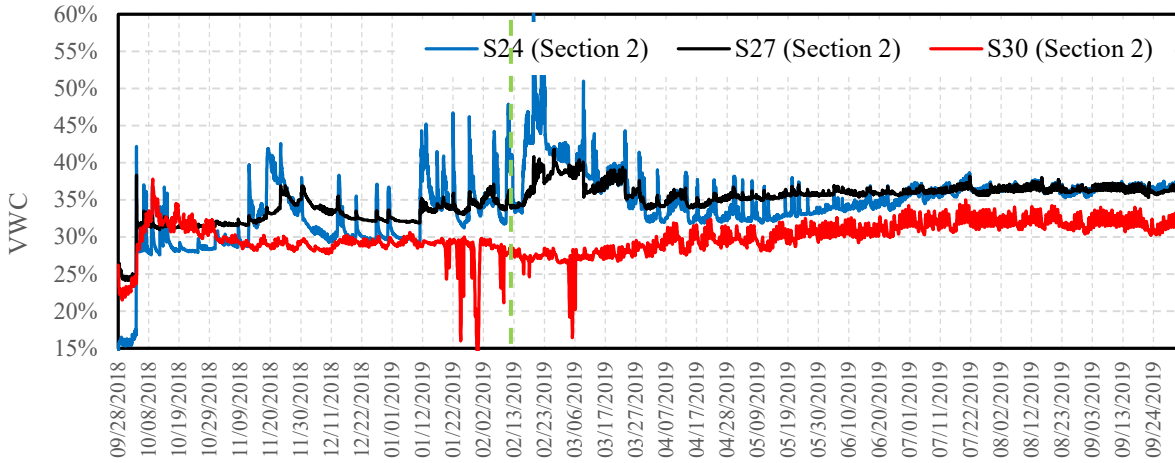


Figure 3.11 Variation of VWC in section 2 at different elevations at the inner edge of the shoulder

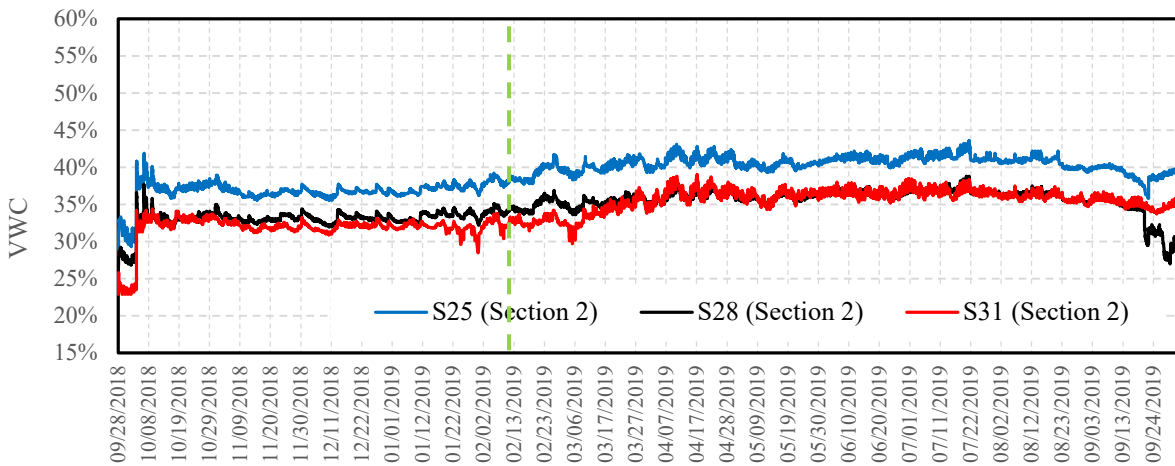


Figure 3.12 Variation of VWC in section 2 at different elevations at the middle of the shoulder

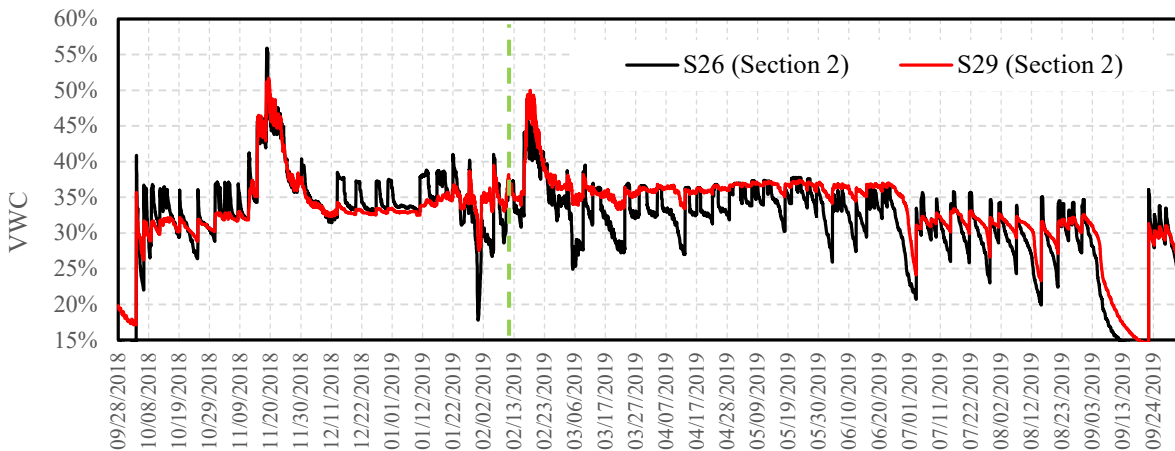


Figure 3.13 Variation of VWC in section 2 at different elevations at the outer edge of the shoulder

Figure 3.14 shows the variations of VWC at the interface between the driving lane and the shoulder in all three sections. The initial moisture content of all of the sensors was around 25%, indicating that the moisture content during the construction was controlled well. Sensors 14 and 17 are located immediately above the wicking geotextile in sections 1 and 2, while sensor 2 was installed at the interface between the subgrade and base course materials. These sensors were at similar locations in different sections.

As can be seen in Figure 3.14, throughout the whole monitoring period, the moisture contents at sensor 30 in section 2 was significantly lower than its counterpart sensors 5 and 17 in the control section and section 1 respectively. This is a clear evidence that the soils at the sensor location were always unsaturated and pumping was unlikely to occur. Similarly, at lower elevations near the interface between the subgrade and base course layer, sensor 27 in section 2 had the lowest VWC most of the time in all three test sections before February 9, 2019, when the wicking geotextile was completely buried. After the exit ends of the wicking geotextile were exposed after February 9, 2019, the VWC at sensor 27 was significantly lower than those at sensor 2 (control) and 14 (section 1), indicating much less likelihood of pumping issues.

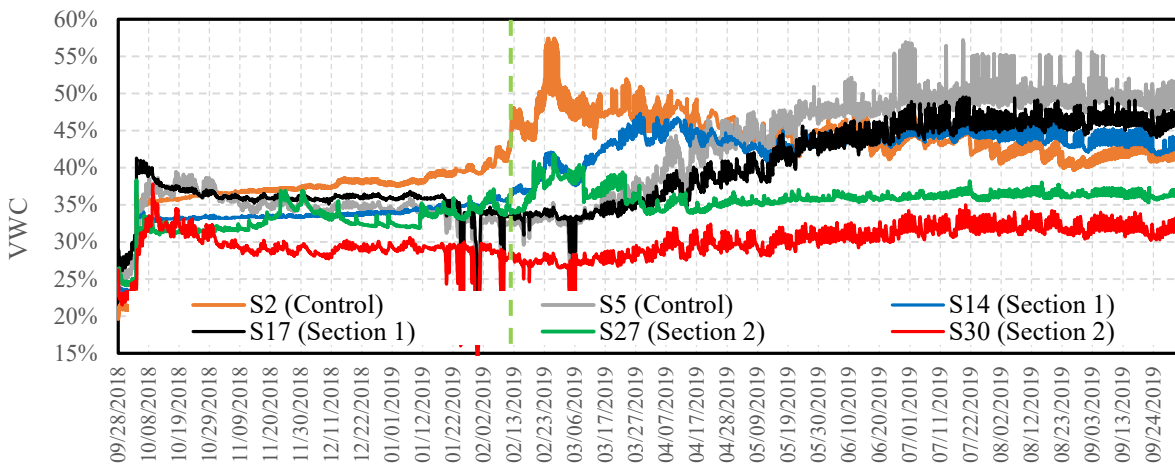


Figure 3.14 Variations of VWC at different elevations at the inner edge of the shoulder

3.6 Contour Plots of Volumetric Water Content at Different Times

In the previous sections, VWC changes at individual sensor locations were presented and compared to evaluate the performance of the three test sections. As discussed previously, due to the variability of the materials and compaction efforts at different elevations, the soils most likely are nonuniform in the constructed test sections, although the research team tried their best to install the sensors with the same soils. As a result, VWC readings at each individual sensor location might not be comparable to each other and are likely to result in misleading or conflicting results. Therefore, it is more important to analyze the test results as a whole instead of focusing on results from each individual sensor.

In order to better evaluate the performance of the three test sections, the VWC readings from all sensors at the same time were presented in a three-dimensional plot using the Matlab program, by generating VWC contours for all three test sections as shown in Figures 3.15 and 3.16. Since the sensors only provided VWC readings for discrete locations, linear interpolation techniques in

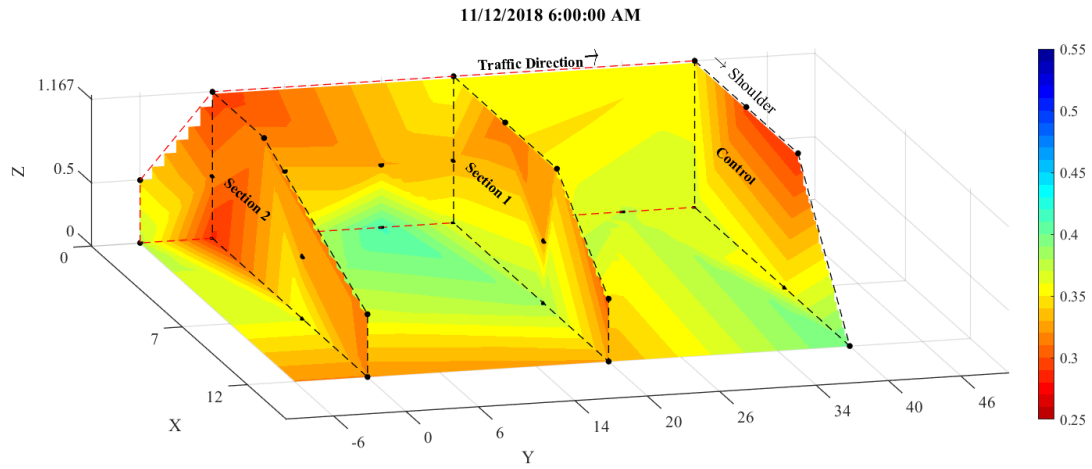
Matlab were used to calculate the VWC at any location of interest and the results were plotted as contours to demonstrate the spatial distributions of water in the test section. Again, it is worth noting that one should look at the overall moisture distributions instead of focusing on VWC at individual sensor locations. Furthermore, the research team put the moisture contours at different times and made a video to dynamically demonstrate the moisture migration in the test section. The video is attached to the report and is available upon request. In this report, only some snapshots were presented to emphasize some key findings during the monitoring period.

The performance of different test sections can be best seen by comparing the VWC contours before, during, and after a rainfall event, which can clearly demonstrate where the water comes from, how it migrates in the pavement structure, and what is the long-term trend. Two rainfall events were analyzed in this report, one is before February 9, 2019, when the wicking geotextiles were completely buried, and another one is a rainfall event after the exit end of wicking geotextiles were exposed to the atmosphere.

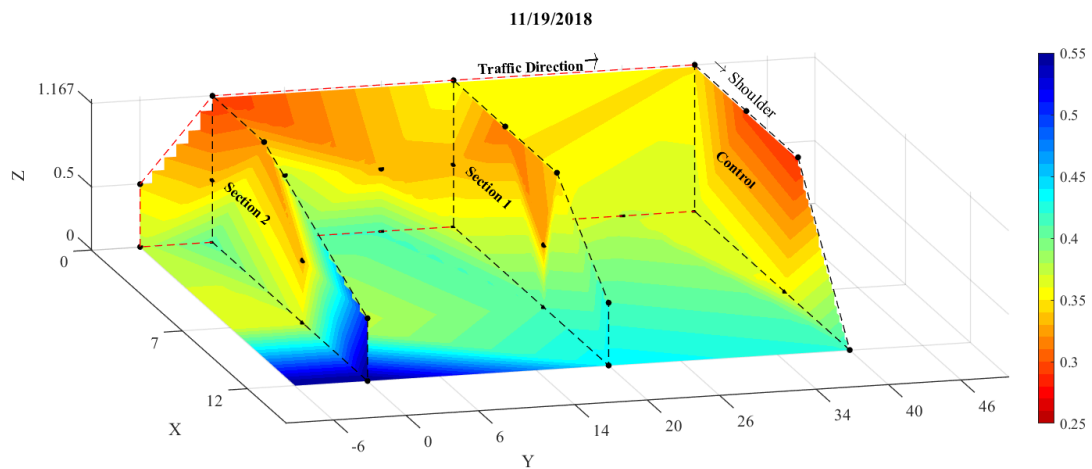
3-6-1- A rainfall event before February 9, 2019

Figure 3.15a shows the spatial distribution of VWC at 6:00 A.M. on November 12, 2018, which is 7 days before the rainfall of November 19, 2018. At least one week had passed since the latest rainfall, and all of the three test sections were relatively dry. It can be seen from Figure 3.15a that section 2 was much drier compared with the other two sections, especially at the interface between the driving lane and the shoulder, where pumping damage was mostly observed. The driest location in section 2 is at the upper part of the interface between the driving lane and the shoulder, which indicated superior performance since if the soil at that point were dry, it is unlikely for the pumping to occur. The soils at the interfaces between the driving lane and the shoulder in section 1 and the control section were relatively dry compared with the soils at the interfaces between the subgrade and base course layer, but wetter than those in section 2 at the similar locations. Another observation was that soils near the surface were drier than soils inside the road shoulder.

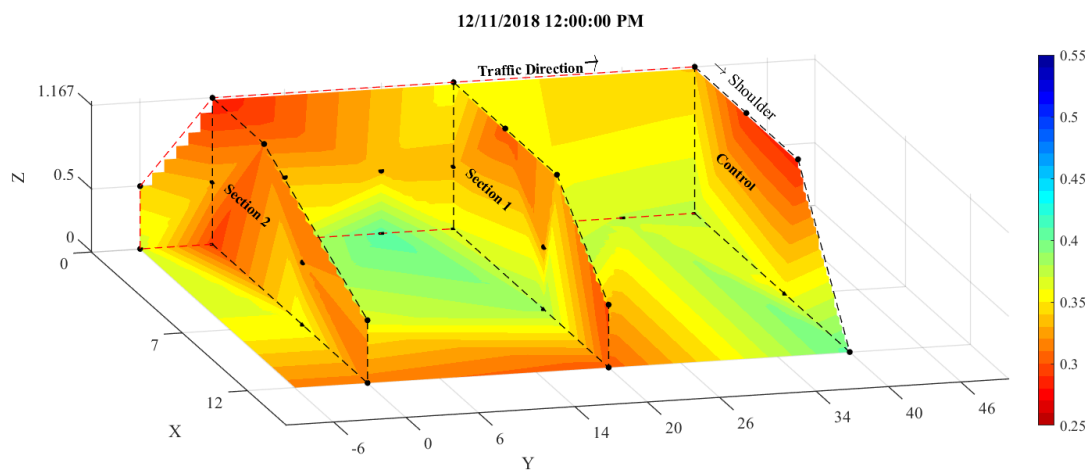
Figure 3.15b shows the spatial distribution of the VWC during a rainfall event of November 19, 2018, with accumulated precipitation of 0.12 in. (3 mm). The VWCs in all three sections increased in general, although the increases at the side slope portion were larger than that inside the shoulder. This is reasonable since it was much easier for the rainwater to infiltrate into soils at the side slope which was not covered by asphalt concrete. The largest increase in the VWC occurred at the side slope of section 2. The increases in the VWC in section 2 were clearly larger at the lower part of the interface between the driving lane and the shoulder than those at similar locations in the control section and section 1. This might be attributed to two reasons. First, water infiltrated preferably downward along the interface between the driving lane and the shoulder and ponded at the corner of subgrade and base course layer interface. In other words, there was a small horizontal distance between the sensor 30 and the vertical interface between the driving lane and the shoulder and water infiltrated more quickly along the vertical interface than flowed horizontally. As a result, sensor 30 recorded less increases in VWC than sensor 24. Secondly, the wicking geotextile in section 2 was wider in the horizontal direction than that in section 1. As a result, water can backflow into the road shoulder more easily during a rainfall event.



(a) Before rainfall on 11/12/2018



(b) During rainfall on 11/19/2018



(c) After rainfall on 12/11/2018

Figure 3.15 VWC at different times before February 9, 2019

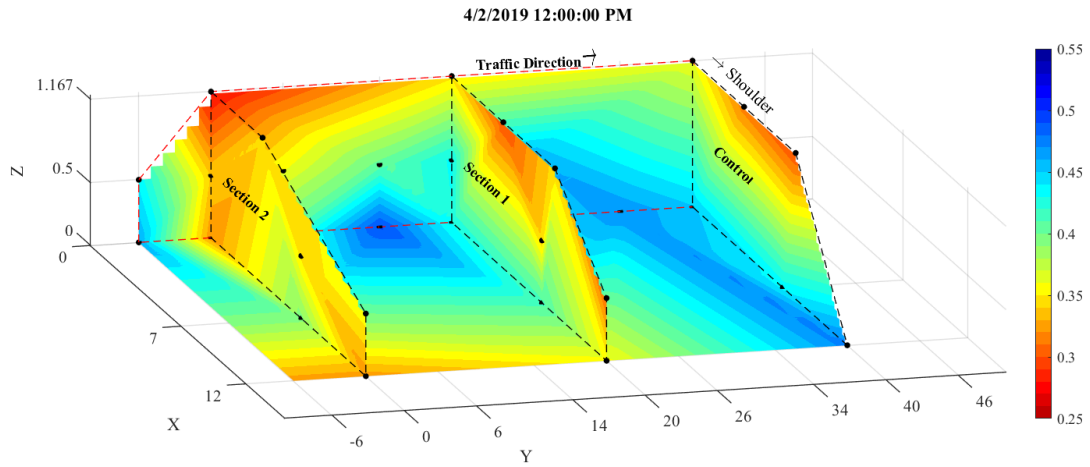
Figure 3.15c shows the distributions of VWC in all three sections on December 11, 2018, which was more than two weeks after the main rainfall event on November 19, 2018. Compared with Figure 3.15b, soils at nearly all locations had lower VWCs in Figure 3.15c. It was found that larger changes in VWC occurred in soils near the surface than those inside the road shoulder, and the largest VWC changes occurred in section 2 at the lower part of the interface between the driving lane and the shoulder. At the similar locations in section 1, there was no visible changes in VWC, while in the control section, there was a slight increase in the VWC. It is therefore concluded that section 2 performed the best, section 1 was the second, and the control section performed the worst in terms of water drainage.

3-6-2- A rainfall event after February 9, 2019

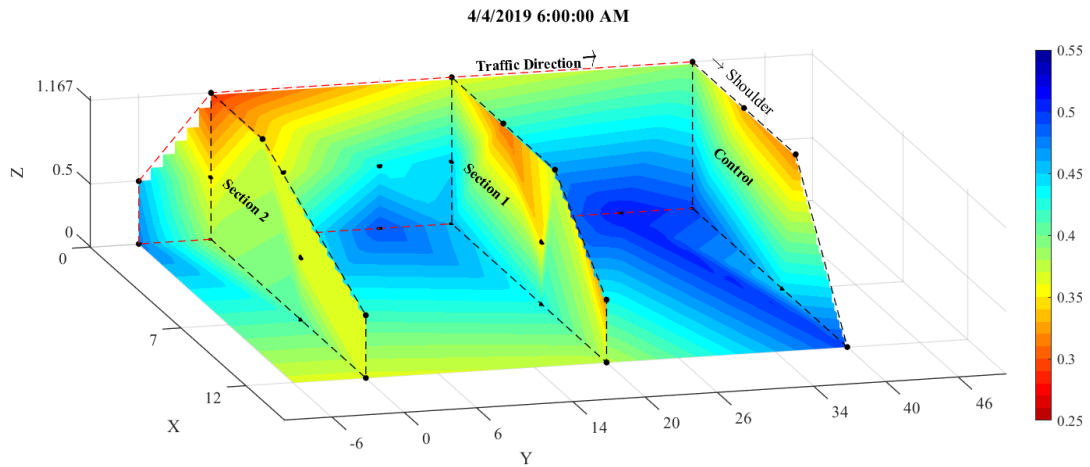
Figure 3.16 shows the distribution of VWC before, during, and after a rainfall event on April 4, 2019, after the exit ends of wicking geotextiles in sections 1 and 2 were exposed on February 9, 2019.

Figure 3.16a shows the distributions of VWC in all test sections on April 2, 2019, which was a few days after the last rainfall on March 30, 2019. In general, the VWCs in all test sections in Figure 3.16a were higher than those at the same locations as shown in Figure 3.15a, indicating that the VWC increased during the spring of 2019 due to some additional rainfall events. Similar to Figure 3.15a, all soils near the surface in Figure 3.16a were much drier than soil inside the road shoulder. In sections 1 and 2, the soils at the interface between the subgrade and the base course layer were drier than inside, especially at the exit side. In contrast, in section 1, the soils at the interface between the subgrade and the base course layer were still fairly wet. At the lower part of the interface between the driving lane and the shoulder, soils at section 2 were fairly dry, some soils at section 1 were fairly wet, and the soils at the whole control section were wet.

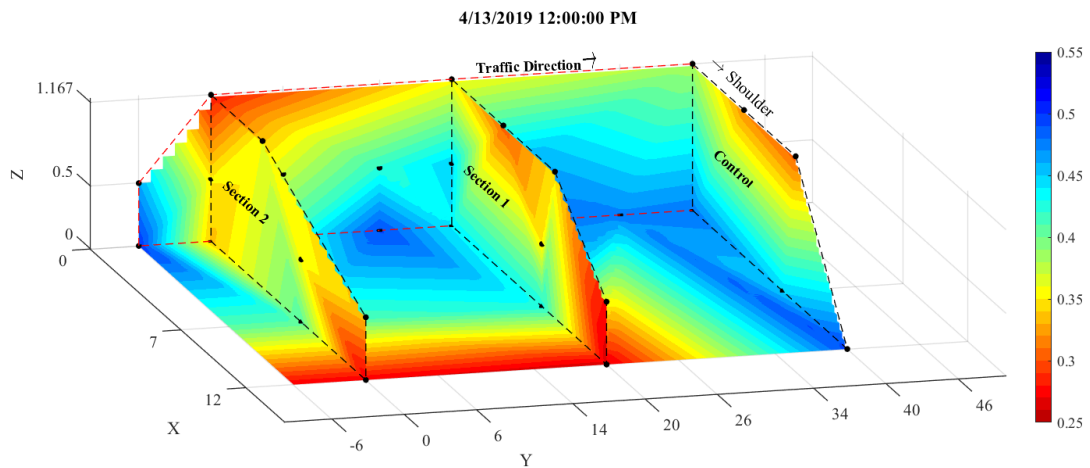
Figure 3.16b shows the distributions of VWC in all test sections on April 4, 2019, during a rainfall event with accumulated precipitation of 0.53 in. (13.4 mm). Comparing Figure 3.16b with Figure 3.16a, it can be seen that VWCs in all test sections increased. However, the increases in VWC in section 2 were not very obvious and the soils at all locations were fairly dry, especially at the interface between the driving lane and the shoulder. There were some visible increases in VWC in section 1, especially at the corner of the two interfaces. However, the whole road should body was still fairly dry. In contrast, there were clear increases in VWC in the control section, especially at the vertical interface between the driving lane and the shoulder and the horizontal interface between the subgrade and the base course layer. It is clear that the control section is more prone to pumping as a result of higher VWC compared with sections 1 and 2. This is another evidence that the wicking geotextile can effectively mitigate the pumping.



(a) Before rainfall on 4/2/2019



(b) During rainfall on 4/4/2019



(c) After rainfall on 4/13/2019

Figure 3.16 VWC at different times after February 9, 2019

Figure 3.16c shows the distributions of VWC in all test sections on April 13, 2019, 8 days after the rainfall. Comparing Figure 3.16c with Figure 3.16b, it can be seen that VWCs in all test sections clearly decreased. The decreases in VWC in sections 1 and 2 were significant at the side slope and at the interface between the subgrade and the base course layer near the side slope. There were some visible decreases in VWC in sections 1 and 2 along the vertical interface between the driving lane and the shoulder. However, it was more obvious in section 2 than in section 1. In contrast, in the control section, although there were some decreases in VWC at the edge of the road shoulder, the soils at the vertical interface between the driving lane and the shoulder and the horizontal interface between the subgrade and the base course layer were still fairly wet. Compared with sections 1 and 2, it is much easier for fined graded soils in the control section to migrate to the base course layer and be ejected out of the pavement structure along the vertical interface between the driving lane and the shoulder, which is pumping.

In a summary, the following conclusions can be made for this section: (1) the moisture content in the pavement structure will increase with time, even if the pavement is constructed under very low moisture content. Longer monitoring time is needed to find out the long-term moisture the road shoulder will reach. (2) Without considering the separation, filtration, and reinforcement functions, the wicking geotextile can significantly reduce the moisture content at the horizontal interface between the subgrade and the base course layer and the vertical interface between the driving lane and the shoulder. This can potentially result in two beneficial effects: (a) it reduces the possibility of migration of fine-grained soils from the subgrade to the base course layer, and (b) it can reduce the likelihood of fines being ejected out of the pavement structure, which is pumping. (3) It is important to expose one end of the wicking geotextile to the atmosphere, which can significantly improve the drainage performance, and (4) it seems that horizontal installation of wicking geotextile performed better than the L-shaped installation for the case in this study.

CHAPTER 4: COMPLIMENTARY TESTS

This chapter presents some laboratory test results on basic soil properties of the base course material used in the I-44 test sections.

4.1 Particle Size Distribution Test

As a basic soil characterization, the base course material was graded using the sieve analysis method. The base course soil originally used for the construction of the test sections contained cobbles and large boulders. Since the permeability of the base course materials mainly depended on the finer particles, the larger soil particles were sieved out using 3/8 in. sieve. The remainder of the soil was used for the particle size distribution test. Figure 4.1 shows the gradation curve of the base course material passing 3/8 in. sieve. Based on the soil particle size distribution, the base course is characterized as poorly graded sand with silt (SP-SM) using the Unified Soil Classification System. The gravel, sand and fine contents were equal to 30%, 60%, and 10%, respectively.

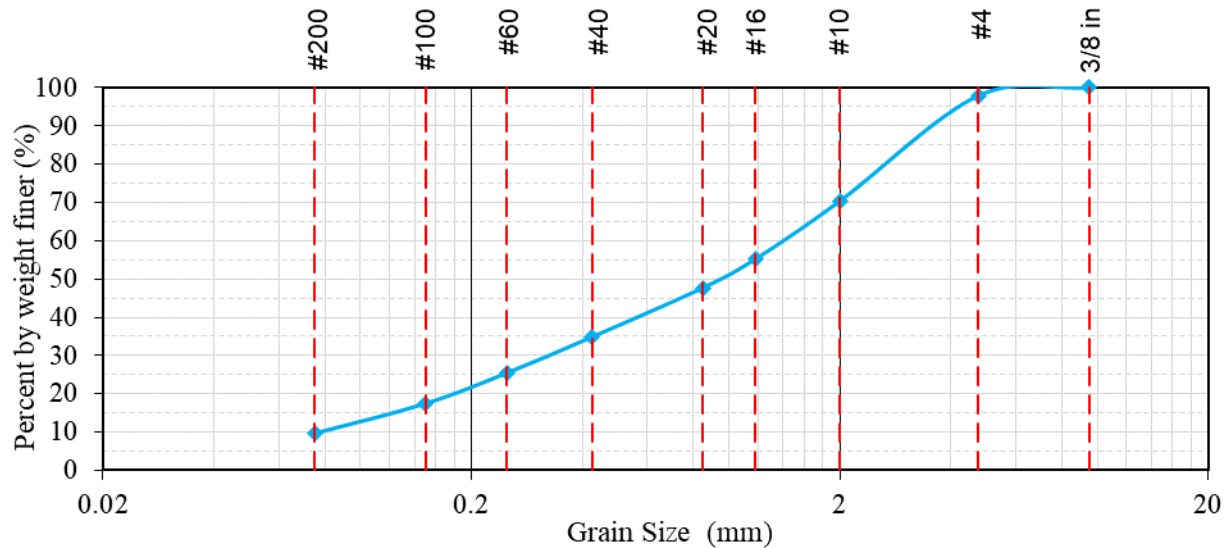


Figure 4.1 Particle size distribution of the base course material passing 3/8 in. sieve

4.2 Briaud Compaction Test

In order to quantify the base course hydraulic conductivity in the lab, firstly, its field density needed to be quantified. The field density of the base course was obtained by correlating the Briaud Compaction Device (BCD) modulus obtained in the lab and the test site. Figure 4.2 shows the application of the BCD test on the test site. Figure 4.3 shows the relation of the density with the BCD modulus, which was obtained by testing compacted soils in the lab. The measured field BCD modulus was used to calculate the dry density of the base course using the results of the laboratory BCD test.



Figure 4.2 BCD field test

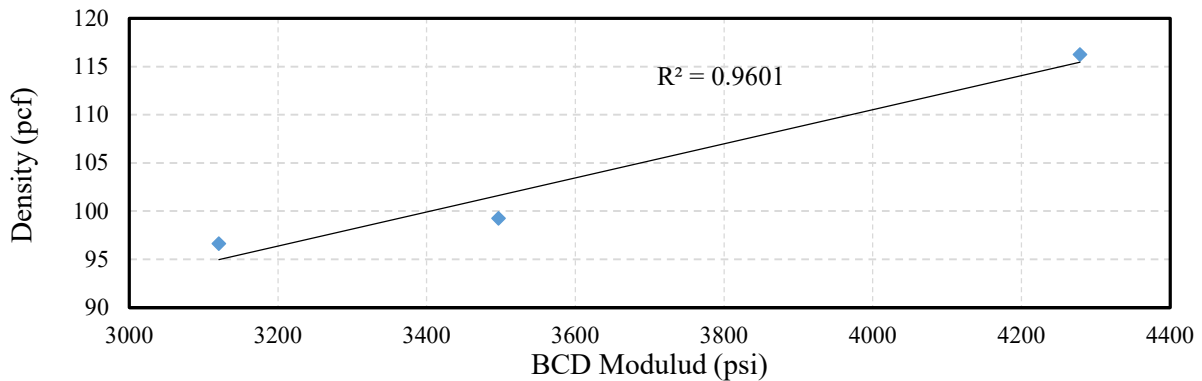


Figure 4.3 Correlation of BCD modulus with soil density for the base course material

Based on the results of the BCD tests, the average BCD modulus of the base course based on several measurements at different locations was approximately 3700 psi (25.5 MPa). The corresponding average density of the base course material in the field was calculated as 106 pcf (16.6 kN/m³). The calculated density was then used to construct the small scale box test in Chapter 5 as explained later.

4.3 Proctor Compaction Tests

The sensitivity of the base course material with respect to its water content was investigated by the proctor compaction test. Figure 4.4 shows the results of standard and modified proctor tests. It can be seen that the maximum dry densities of the base course are 135 pcf (21.2 kN/m³) and 137 pcf (21.5 kN/m³) for standard and modified proctor tests, respectively. The corresponding optimum water contents were approximately 7.4% and 9%, respectively.

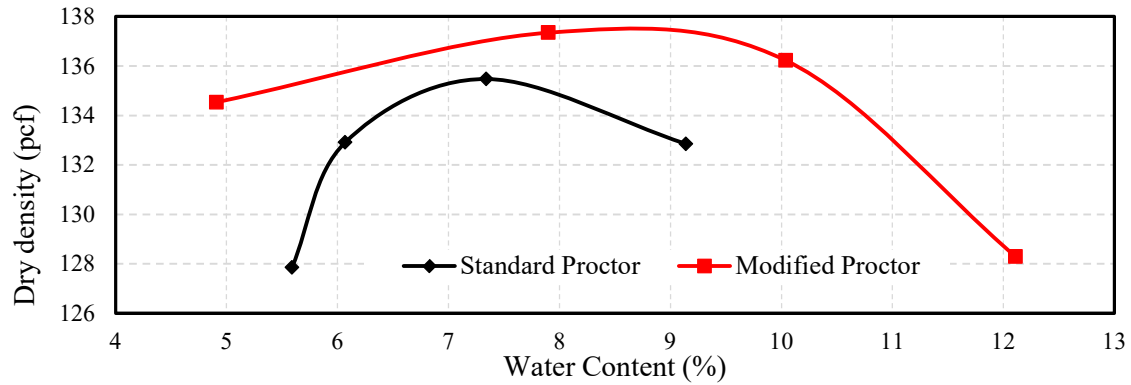


Figure 4.4 Compaction test results

4.4 Laboratory Hydraulic Conductivity Test

Hydraulic conductivity tests in saturated conditions were performed both at field density and maximum dry density of the base course material passing 3/8 in. sieve. The constant head hydraulic conductivity test was used to measure the hydraulic conductivity of the tested soil at the field density, whereas the falling head hydraulic conductivity test was used to measure the hydraulic conductivity of the soil at its maximum dry density. The measured hydraulic conductivity at field density of the soil (k) was 0.005-0.01 cm/s. For the soil compacted at its maximum dry density of 137 pcf using modified proctor test procedure, the measured hydraulic conductivity using the falling head test procedure was $2.2-2.4 \times 10^{-8}$ cm/s.

CHAPTER 5: SMALL SCALE BOX TEST

In order to study the effect of the installation of the wicking geotextile in the base course soil in a more controlled setting, a series of small-scale box tests were performed. This chapter explains the experimental setup, instrumentation, experimental design, and results of the different tests.

5.1 Experimental Setup

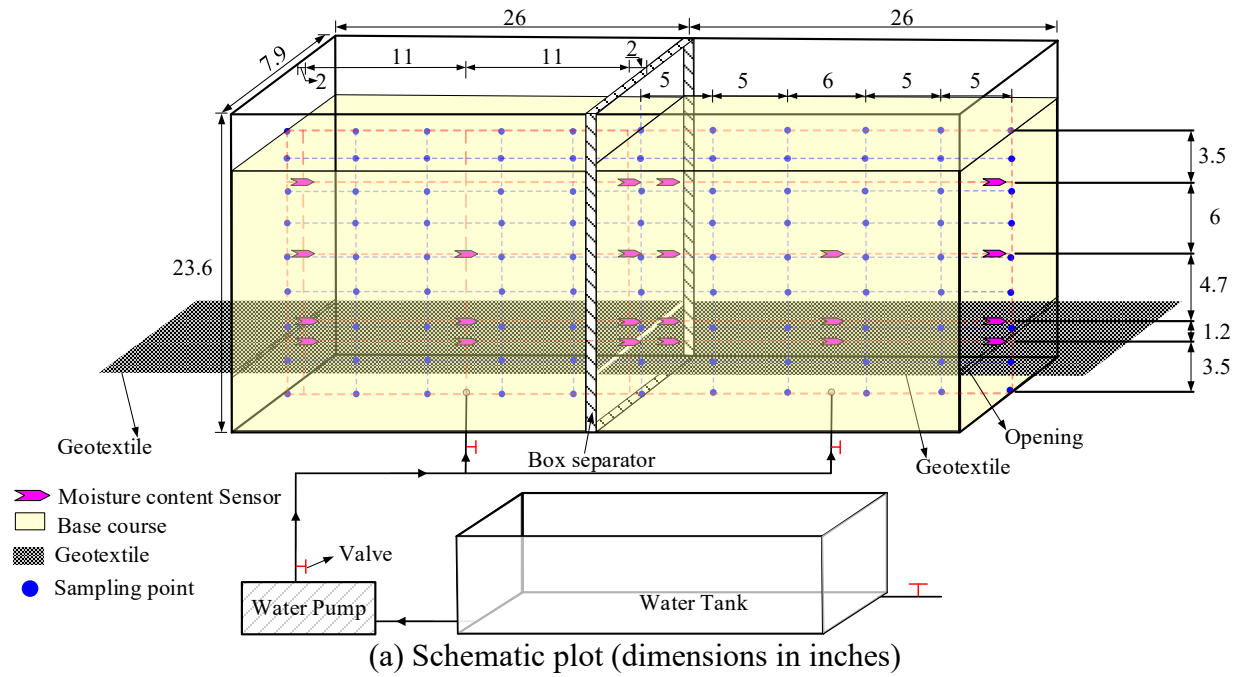
Figure 5.1a and 5.1b show the configuration of the experimental testing box. The testing box frame was built with aluminum alloy to provide strong support for the testing materials. The sidewalls were made of transparent acrylic to facilitate the observation of the moisture migrations within the testing box. The dimensions of the testing box were 52 in. \times 23.6 in. \times 7.9 in. (132 cm \times 60 cm \times 20 cm) (Length \times Height \times Width). In order to compare drainage efficiency of different geosynthetics at the same time, the test box was divided into two sections, the dimensions for those two sections were 26 in. \times 23.6 in. \times 7.9 in. (66 cm \times 60 cm \times 20 cm) (Length \times Height \times Width), respectively, as shown in Figure 5.1a.

The soil used was the same soil used in the construction of the field test section. However, only the soil particles passing 3/8 in. sieve were used to build the experimental sections. In all tests, the soils were compacted to a height of 18.9 in. (48 cm) with an initial dry density equal to the measured field density ($\gamma=106$ pcf) using 1.2 in. (3 cm) lifts. The corresponding saturated coefficient of permeability of the soils was 0.005-0.01 cm/s. Two valves were installed at the bottom of the left and right side of the box for water supply. Meanwhile, there were two openings (7.9 in. (20 cm) (W) \times 0.08 in. (2 mm) (H)) located at each side of the sidewalls of the test apparatus with an elevation of 3.9 in. (10 cm) from the bottom. These openings were designed to install the drainage materials. Rectangular grids with dimensions of 1.2 in. \times 1.2 in. (3 cm \times 3 cm) were marked on the front acrylic wall to facilitate the visual observations of the drainage performance.

5.2 Instrumentation

METER Environment® EC-5 Moisture sensors were installed in the testing box to monitor the drainage performance of different materials. In total four layers of soil moisture sensors were installed at depths of 3.5 in. (9 cm), 4.7 in. (12 cm), 9.4 in. (24 cm), and 15.4 in. (39 cm) from the bottom, respectively as shown in Figure 5.1a. The first layer of sensors (3.5 in. from the bottom) was installed at the level of opening and immediately below the wicking geotextile (if there is). In each test section, there were three sensors in the first three layers. In the fourth layer, only two sensors were installed as shown in Figure 5.1a. As a result, in total 11 sensors were installed in each test section as shown in Figure 5.1a. Within each layer, the spacing between two adjacent sensors was 11 in. (28 cm), and the sensors at the edges were 2 in. (5 cm) away from the sidewalls. Note that a $\pm 2\%$ accuracy of the sensor was provided by the manufacturer for non-uniform soils and general field conditions, which represent accuracy under disadvantageous field conditions. In this study, the sensors were used in a well-controlled and stable laboratory condition with nearly constant temperature, relative humidity, nearly zero vibration, and very short connection wires. In addition, the soils used were relatively uniform and were carefully prepared. Therefore, the sensors should be able to provide sufficient accuracy of the soil

moisture variations with time during the tests. In addition, after the test has been completed, a total of 54 samples were taken from each testing box. The volumetric water content was back-calculated based upon the measured gravimetric water content and the specific gravity of the soil. It was found that the monitored and calculated results matched well with each other, indicating that the sensor readings were reasonable and accurate. This can be considered as an indirect calibration. The data acquisition system was composed of a Campbell Scientific® CR1000 datalogger together with an AM16/32 multiplexer. The soil volumetric water contents were monitored and recorded every 2 minutes.



(b) Filled test box

Figure 5.1 Test apparatus

5.3 Experimental Design

To evaluate the performance of the different drainage designs, four cases of drainage tests were performed in the testing box as shown in Figure 5.2. Case I represents the control case where no additional drainage elements were placed in the box. Case II represents a case where a 7.9 in. wide wicking geotextile was placed horizontally at the height of 3.9 in. Case III was similar to Case II. However, the end of the wicking geotextile was folded upward and extended vertically for 11.8 in. at the far side from the outlet. In Case IV, a French drain system was used to drain water from the soil as shown in Figure 5.2. A French drain is usually constructed by placing a perforated pipe wrapped with a nonwoven geotextile to prevent clogging. The pipe is usually buried in a ditch surrounded by gravel to drain subsurface flow. In this study, a 3-in. diameter perforated pipe wrapped by a conventional nonwoven geotextile was placed on top of a gravel bed extending to the opening of the box. The material used for the gravel bed was clean gravel particles passing 1 inch and retaining on top of $\frac{3}{4}$ inch sieve. The gravel bed was placed at 1.5% grade toward the opening with a thickness of 1.2 in. (3 cm) to collect and transport water to the outlet. French drains in practical applications consist of only a perforated pipe wrapped with geotextile to collect water. The water then is transported through a series of crossing pipes in the transverse direction. Since placing a crossing pipe to collect water in a small test box is not practical, a gravel bed was used instead. It should be noted that since the gravel bed is in direct contact with the soil, water can be collected from the adjacent soil directly, along with the collected water in the main perforated pipe. In this way, the drainage performance of the whole system is better compared with those in real applications.

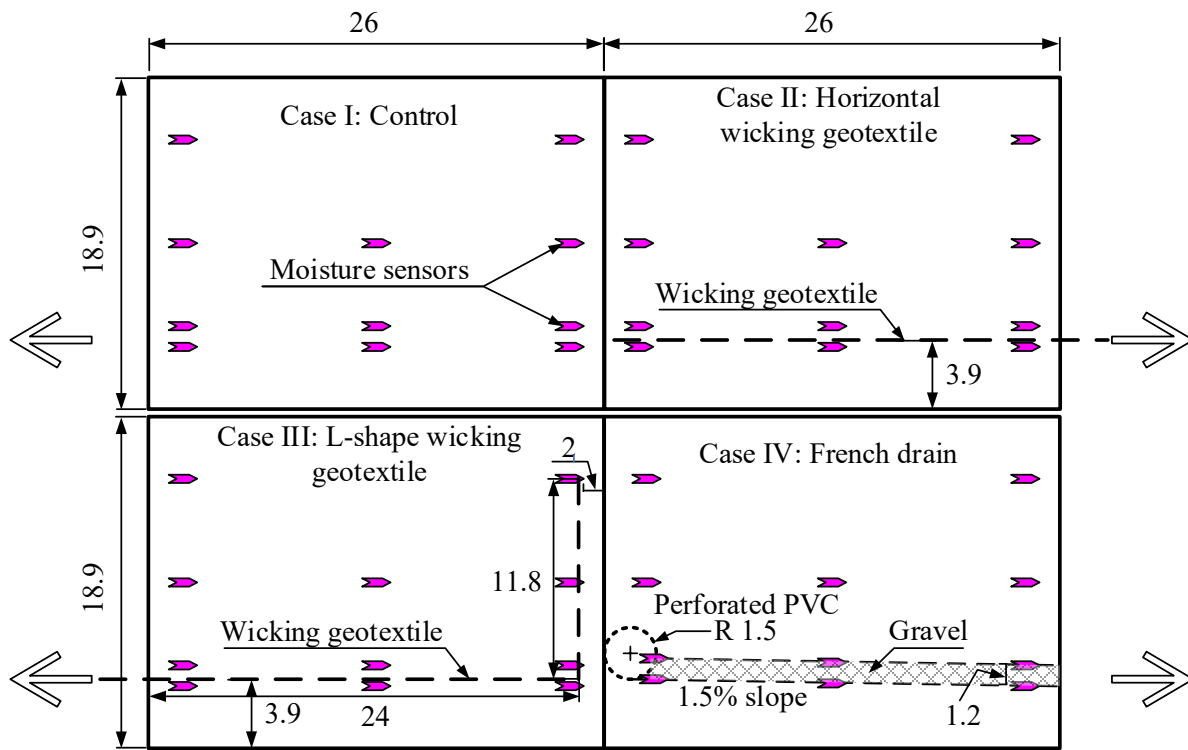


Figure 5.2 Test setup for four different cases and typical sensor arrangement. Case I: control

case with no drainage, Case II: Horizontal wicking geotextile, Case III: L shaped wicking geotextile, Case IV: French drain (dimensions in inches)

5.4 Test Procedures

All tests were carried out in the temperature and humidity-controlled room. The relative humidity varied from 48% to 58%, with an average value of 53% and the temperature varied from 19 °C to 22 °C, with an average value of 21°C. Each test had three different stages. At the first saturating stage, the soils in the entire testing system were saturated. During this stage, water was slowly supplied to the testing box through two valves at the bottom of the box (refer to Figure 5.1b), and gradually saturated soils from the bottom to the top. The water flow rate was carefully controlled to prevent upward seepage force from disturbing the tested soils. The soils were considered fully saturated after a 1 in. water head was ponding above the soil surface.

After the saturation process was completed, the valves at the bottom of the testing box were shut down and the second stage of free draining started. Water was allowed to be drained out of the system through the opening which is shown by an arrow in Figure 5.2. Then the top of testing box was covered by plastic wrap to prevent any possible water loss through evaporation. The wicking geotextiles (if there were), were naturally hung downwards by gravity.

The second stage of the test was completed when there were no visible water drops could be observed. At the third stage of draining capillary water, the wicking geotextile (if there was) was continued to be exposed to the room atmosphere until the exposed end of it was dried. During the entire three draining stages, the soil volumetric water contents were monitored every 2 minutes by the installed sensors.

After all the three stages were completed, the testing system was disassembled and soils at different locations were carefully sampled to measure their gravimetric water contents using the oven method. The solid points in Figure 5.1a show the locations of the sampling. From the top to the bottom, a total of 9 layers of soils were sampled with an interval of 2.4 in. In each layer, six locations were selected for sampling and the sampling distance between two adjacent locations were 5, 5, 6, 5, and 5 in. (refer to Fig. 3a), respectively. As a result, a total of 54 samples were taken for each test section and a total of 108 gravimetric water contents were measured for the whole testing box for two test sections.

5.5 Results and Discussions

In this section, the volumetric water content changes during all cases are presented and discussed. For all cases, approximately after 5 hours, readings from all sensors became constant. As a result, only the first 5 hours data was shown for all cases to make the results more readable. To make the comparison simpler, the readings at the same elevation were averaged to demonstrate the moisture content distributions with elevation. The recorded data was also used to generate the volumetric moisture contours to facilitate the visualizations of spatial water migrations under each situation. Some snapshots were shown at different times to facilitate the discussions.

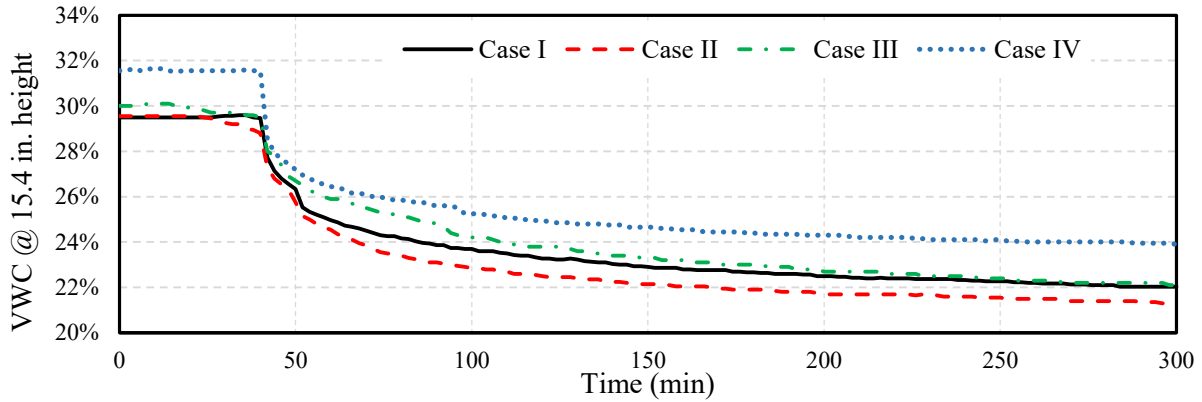
5-5-1- Volumetric water content changes at different locations

Figure 5.3 shows the average volumetric water content readings in the first 5 hours of the drainage tests for each case at heights 3.5, 9.4, and 15.4 in. from the bottom of the test box corresponding to first, third, and fourth layers of sensors, respectively. It is clear that the VWC changes in all of the cases have a similar trend. Initially, the soil was saturated and the sensor readings ranged from approximately 29% to 32%. The difference in the readings is due to the difference in compaction of the soil at different locations, even though a lot of effort was made to compact the soil uniformly. At the time of 20 minutes, the outlets were opened and water started to flow out of the system and the water table in the box started to drop. At the top-level sensors, a sudden drop in VWC was at the time of 40 minutes indicated that the water table reached the depth of 3.5 in. 20 minutes after the opening of the outlet. The average VWC at the top sensors in Case I and Case II started at the same value. However, shortly after 50 minutes, they clearly diverged and the VWC for Case II was always lower than that of Case I. It means that compared with the control case, more water was drained when a layer of wicking geotextile was installed horizontally. The distribution of VWC in Case III was very similar to Case II since in both cases the wicking geotextiles were installed as the drainage materials. VWC at the beginning of the Case IV started slightly below 32% and ended at approximately 24% with a similar trend as Case I. The drops in VWC readings in Cases I and IV were quicker than those in Cases II and III at the same time. The quicker drops in VWC in Cases I and IV indicate that water was drained faster in these two cases at the very beginning stages. This is reasonable since in Cases II and III, where a layer of wicking geotextile was used as drainage materials, part of the area of the outlet was occupied by the geotextile material which slowed down the water flow.

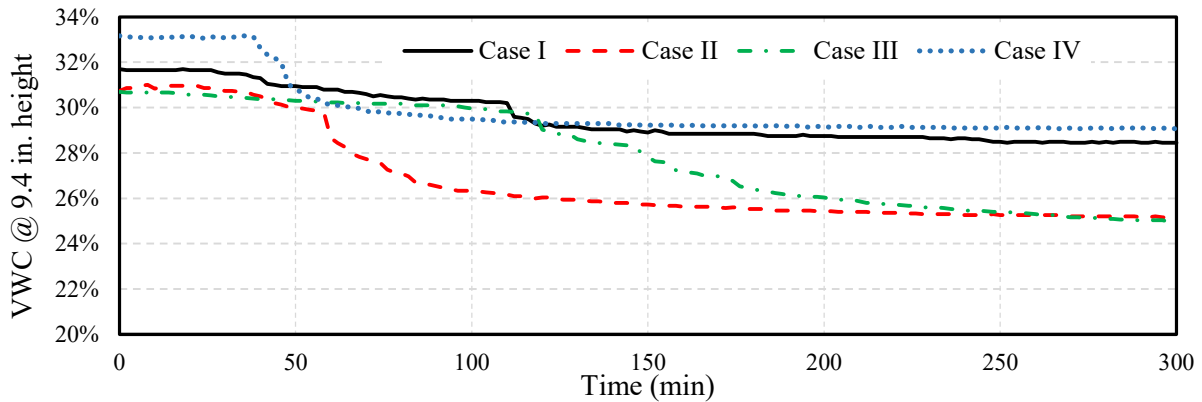
Figure 5.3b shows the average VWC of the third layer of sensors from the bottom. It can be seen that the VWC at the beginning of the test in both Cases II and III started at around 31% and ended at 25%. At the same height, the VWC in Cases I and IV started around 32% and 33% and ended around 30% and 31%, respectively. The difference in VWC at the beginning of the test compared to the end of the test in Cases II and III was 6%. While for Cases I and IV, the difference was about 2%. This clearly indicates that compared with the control case (Case I) and the case with French drain (Case IV), when wicking geotextile was used, more water can be drained out of the test box (representing the pavement structure).

Comparing Case I and Case IV at different elevations shows that the difference in the VWC readings was minimal and the two cases performed similarly. The reason for the similar performance is that the permeability of the base course used in this study at the current degree of compaction was relatively high. During the tests for Cases I and IV, the soil above the opening was saturated only for a short time. After the soil became unsaturated the permeability of both Control and the French drain dropped significantly and reached almost zero. As a result, water could not effectively be drained out of the soils under unsaturated conditions, thus the performance of the French drain and the base course was essentially limited.

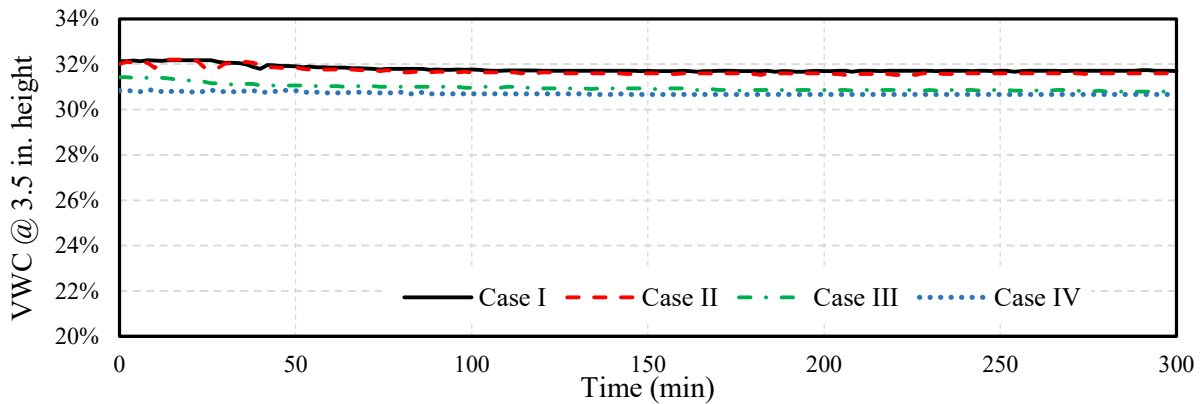
Figure 5.3c shows the average VWC at the first (lowest) layer of sensors in the four cases. As seen in Figure 5.3c, all of the sensors maintained a relative constant reading of 31-32%. It is clear that the soil in all cases was still in the saturated condition at the height of 3.5 in., which is below the elevation of the opening.



a) Fourth (top) layer of sensors (h = 15.4 in. from the bottom)



b) Third layer of sensors (h = 9.4 in. from the bottom)



c) First layer of sensors (h = 3.5 in. from the bottom)

Figure 5.3 Average VWC for different cases

In order to eliminate the influences of possible nonuniform soil compaction, the VWC results were normalized by comparing the VWC changes relative to their corresponding initial VWC. This is helpful since the differences in the initial saturated VWC is mainly due to the difference in compaction of the soil at different locations. The results are illustrated in Figure 5.4. It is clear that Case II was the driest for the most part except at the beginning of the test. Case III had a similar trend to Case II. At the end of the fifth hour, Case I had the highest VWC. The difference

between sensor readings of the four cases was insignificant since the top portion of the soil was far from the drainage outlet and the VWC was mainly affected by the soil permeability and availability of water, which for all of the cases was the same.

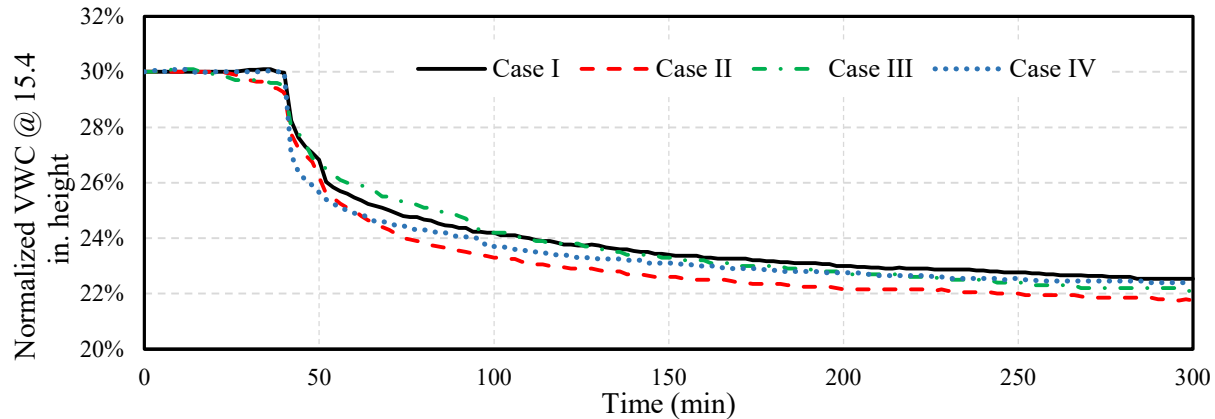


Figure 5.4 Normalized average VWC for different cases at top sensors ($h = 15.4$ in.)

5-5-2- Volumetric water content contours at different times

Figures 5.5 through 5.7 show the contour plots of VWC at different times for each case. These contour plots were generated by linearly interpolating the VWC at different sensor locations to obtain a continuous spatial distribution of moisture content. In each figure, the arrow in the bottom left corner shows the location of the opening.

Figure 5.5 shows the VWC distribution at the beginning of the tests after saturating soils in the box. It can be observed that all of the sensor readings showed a value of 30-32% that fell within the accuracy of the sensors. However, the VWC sensor below the French drain pipe showed a higher value since it was directly in touch with soils with larger voids in the gravel bed and the French drain pipe itself.

Visual observation during the tests showed that the initial water discharge from the opening was high for all cases. Within the first 3 hours, most of the gravity (“free”) water was drained out in all cases. Figure 5.6 shows the distribution of VWC after 3 hours when all of the free water has been drained out. As shown in Figure 5.6, the VWC contour lines for Case I are relatively horizontal. The lower values of the VWC at both sides of the box could be attributed to the boundary effects since water could flow more easily at the soil-wall interface. The saturation VWC (30%) line in the contour was located at the elevation of approximately 7.1 in. from the bottom of the box, indicating the capillary rise was 3.1 in. In Case II, the wicking geotextile was installed horizontally at an elevation of 3.9 in., as illustrated by the dashed line in Figure 5.6. Similar to Case I, the VWC contour lines were relatively horizontal at the lower levels with a slight inclination to the far side of the opening at higher elevations. In contrast to Case I, the 30% VWC contour line in Case II was lower and was located at a height of approximately 5.5 in. This was the result of improved drainage performance caused by using a layer of wicking geotextile at the height of 3.9 in. In Case III, it can be seen that the saturation water content line was lower than those in other cases and was located at a height of 3.9 in. It should be noted that all of the contour lines on the left side of the box are inclined towards the outlet. However, on the right

side at the locations adjacent to the vertical part of the wicking geotextile, these lines are perpendicular to the wicking geotextile. This is an indication that the hydraulic gradient around the wicking geotextile is larger, causing a change in contour line inclination. The contour lines in Case IV are inclined towards the outlet on the left side and toward the PVC pipe on the right side of the box. This is expected since both of these locations acted as an outlet due to the existence of large voids and a large portion of free water was collected directly at those locations.

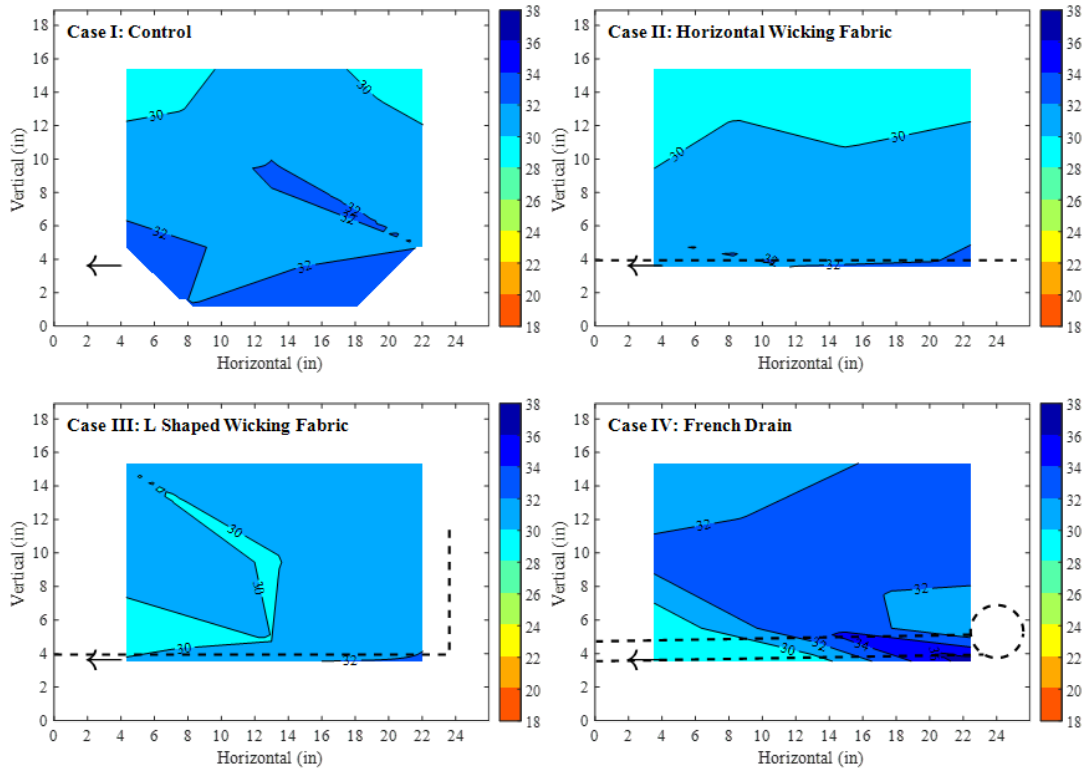


Figure 5.5 Distributions of VWC in all four cases at initial condition (VWC in percentage)

Figure 5.7 shows the contour plots for all cases 2 days after the beginning of the test. Although the tests were continued for 7 days, after 2 days, all the sensors measured no further change in VWC. The general trend of VWC lines was similar to Figure 5.6. However, the VWC distribution indicates that some water drained out even after all of the free water had been drained. This extra water drainage was considered mainly the capillary water. Comparing Figure 5.5b with 5.5c, it can be clearly seen that more water was drained in Cases II and III. On the other hand, the changes in VWC in Cases I and IV were trivial during the period. This clearly indicates that wicking geotextile was continuously draining the capillary water at a higher rate. As shown in Figure 5.3c, in terms of drainage performance, Cases II and III were clearly better than Cases I and IV. It can also be seen from Figure 5.3c that compared with the control case I, adding French drain to the soil slightly improved the drainage performance of the system, but was less significant compared with the cases with the wicking geotextile. These results verified that installing the wicking geotextile has a beneficial effect on draining extra capillary water out of the pavement structure.

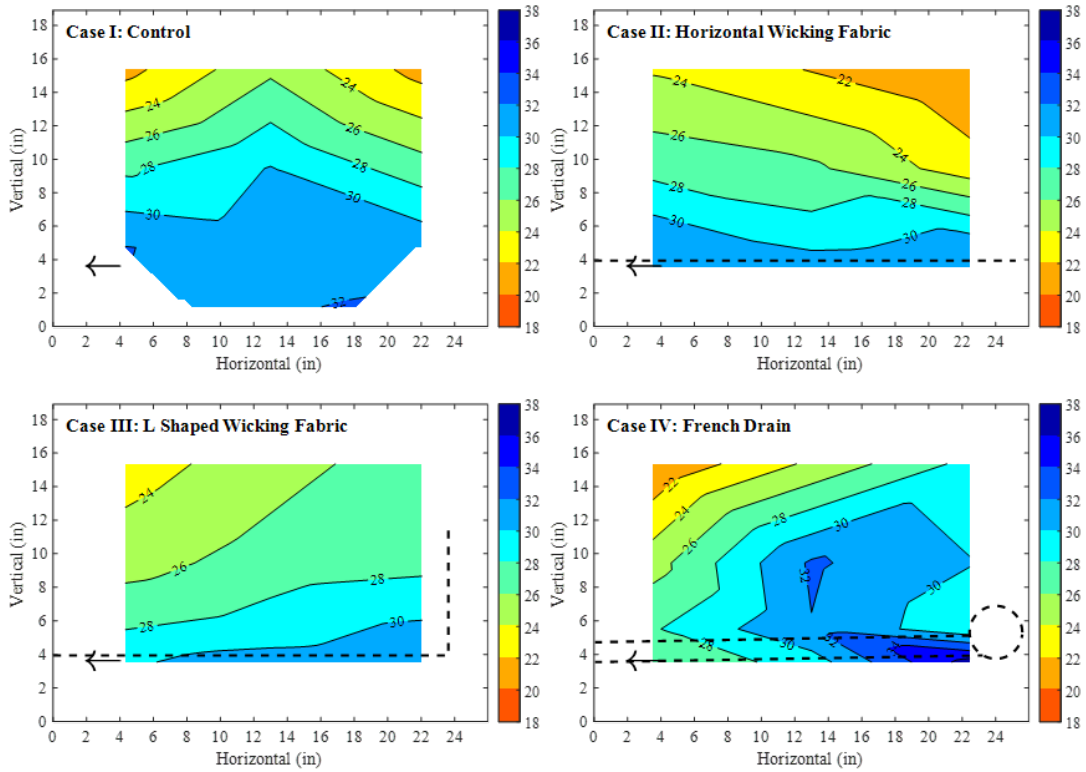


Figure 5.6 Distributions of VWC in all four cases after 3 hours (VWC in percentage)

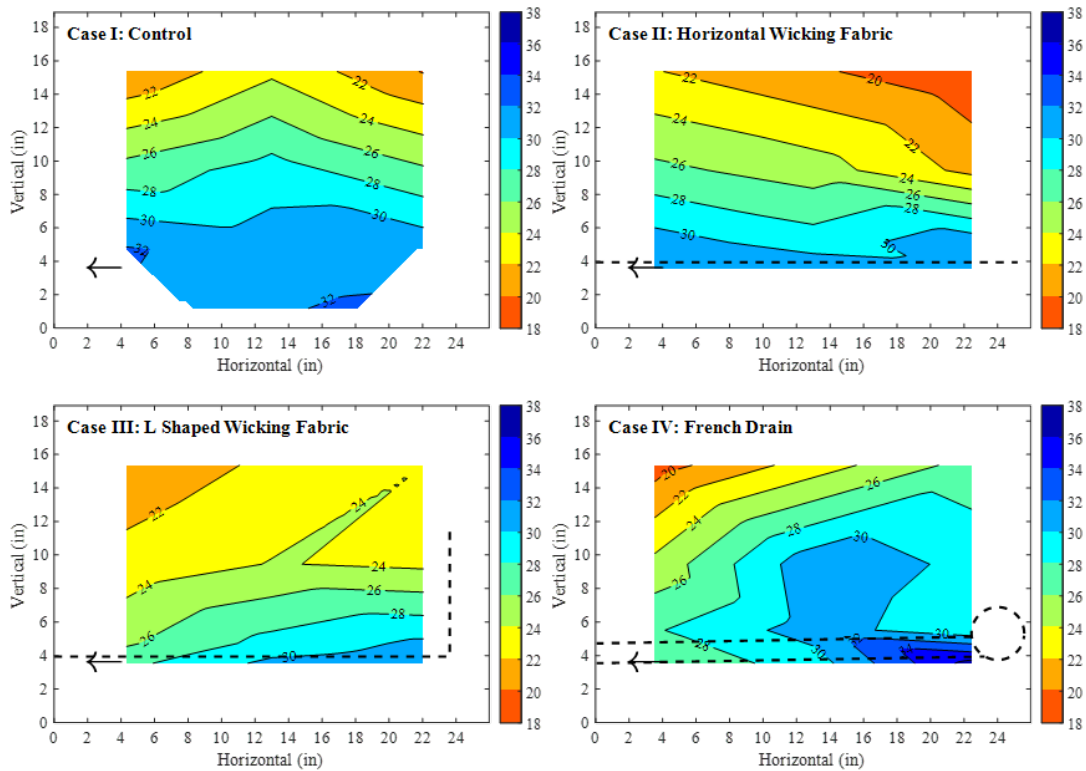
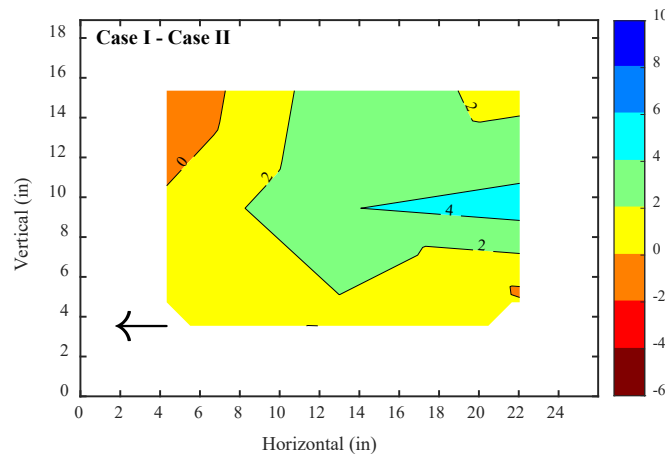


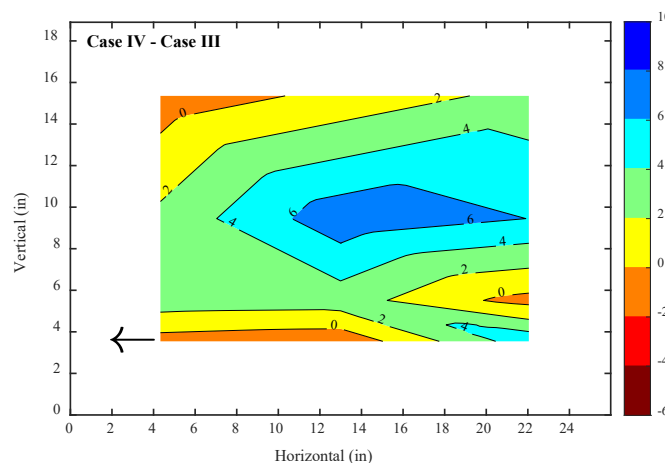
Figure 5.7 Distributions of VWC in all four cases after 2 days (VWC in percentage)

To better demonstrate the differences in drainage ability of different cases, Figure 5.8 shows the differences in VWC distributions between Cases I and II, and Cases IV and III after 2 days of draining. VWC in Case II was subtracted from the VWC in Case I and the results were shown in Figure 5.8a. As shown in Figure 5.8a, immediately above the location of the opening (3.9 in.), the differences in VWC between Cases I and II were negligible. The reason for this is that the soil at the elevation of the opening in all cases is nearly saturated, and the wicking geotextile did not improve the drainage when the soils are fully saturated. Since the soil used in this case has high saturated hydraulic conductivity, the beneficial effect of the wicking geotextile is shadowed. On the other hand, at the height of 9.4 in. (5.5 in. above the wicking geotextile), a reduction of VWC up to 4% more compared with the control case was observed. The relative contour values at the top of the soil are close to zero showing that no significant improvement observed at this elevation.

Similarly, VWC in Case IV was subtracted from the VWC in Case III and the results were shown in Figure 5.8b. At the elevation level that is close to the outlet, the two systems generally performed similarly as indicated by contour line with values close to zero. On the other hand, at the mid-height of the box, wicking geotextile reduced VWC up to 6% more than the French drain, indicating the efficiency of the wicking geotextile in draining water.



(a) Case I minus Case II



(b) Case IV minus Case III

Figure 5.8 Relative VWC after 2 days.

CHAPTER 6: CONCLUSION

In this study, a new type of wicking geotextile was used to mitigate pumping in pavements in Missouri. A field test site was constructed at milepost 117.2 of eastbound Interstate 44 in Missouri. In order to compare the different placements of the wicking geotextile in reducing moisture content in the pavement, the test site includes three sections. One is the control section without wicking geotextile, section 1 is a section with L-shaped wicking geotextile, and section 2 is a section with horizontal installation of wicking geotextile. Construction of the test site finished on September 27, 2018, and all test sections were instrumented with moisture sensors. At the time of submission of this report, the test site has been monitored for one year. The test results clearly demonstrated that the installation of wicking geotextile had significantly reduced the moisture content in the pavements structure and was beneficial to the mitigation of the pumping issue. Some small-scale laboratory tests were also performed to investigate the drainage performance of wicking geotextile in a more controlled environment. The laboratory test results were consistent with the field monitoring results. Below are some findings from the field test monitoring results:

1. Although the road shoulder was constructed at very low initial moisture content, the moisture contents in the road shoulder quickly increased to a high level after the first rainfall. Although the road shoulder was constructed with granular materials with high permeability, the excess water, which is mainly capillary water, cannot be drained out through conventional drainage systems such as French drain. In the control section, the moisture content remained at a higher level throughout the monitoring period. The soils may become nearly or completely saturated if water is not drained quickly after a rainfall event. Numerous studies have indicated excess water is the major reason for pavement distresses and pumping.
2. Moisture contents in all three test sections in the road shoulder constantly changed with the local climatic conditions. Rainfall infiltration was the major reason for moisture content increase, and which occurred quickly after the rainfall event. Moisture content reduced slowly due to lateral drainage and evaporation after a rainfall event.
3. Installation of a layer of wicking geotextile successfully drained more water from the pavement and provided a drier system compared with conventional systems like French drains.
4. Exposing the end of wicking geotextile to the atmosphere significantly increased the drainage performance. The wicking geotextile worked a high efficient “pipe”, and the lower than 90% relative humidity in the atmosphere is the “pump” which provided the driving force for the moisture migration.
5. During rainfalls, water could backflow into the pavement from the exposed end of the wicking geotextile for a short period. However, shortly after rainfall stopped, wicking geotextile drains water out of the soil.
6. In all three test sections, section 2 with horizontal installation of wicking geotextile performed the best. section 1 installed with L-shaped wicking geotextile performed much better than the control section, but not as good as section 2.

7. The reduction in VWC by using wicking geotextile was up to 6% in the laboratory tests and up to 10% in the full-scale field tests.

8. The overall VWC in the field sections were higher in spring than winter. The reduction in VWC in spring was up to 10%. However, at the same point, the reduction of VWC was 5% during winter times.

9. This study did not directly address the separation/filtration behavior of the wicking geotextile. It has been shown that wicking geotextile successfully drained capillary water in pavements and increased suction in soil. This is beneficial in mitigating pumping since even under repeated traffic load, the pore water pressure would not reach positive values that can result in fines migration and pumping. Thus, pumping and potential clogging would not occur. Literature review of previous studies indicated that clogging of the wicking geotextile was not a concern in the long term.

Finally, it is worth noting that the test site was completed within a year and the conclusions were based on the test results of limited monitoring time. As it was discussed before, pumping is a gradual process that occurs over a long time. The long-term performance of the wicking geotextile to mitigate pumping issues still needs to be further explored. It is suggested that the test sections be monitored for a longer period to evaluate the long-term performance of wicking geotextile to mitigate pumping issues.

REFERENCES

- Abu-Farsakh, M., Hanandeh, S., Mohammad, L., and Chen, Q. Performance of geosynthetic reinforced/stabilized paved roads built over soft soil under cyclic plate loads. *Geotextiles and Geomembranes*, 2016. 44(6): 845–853.
- Al-Qadi, I. L., Brandon, T. L., Valentine, R. J., Lacina, B. A., and Smith, T. E. Laboratory evaluation of geosynthetic-reinforced pavement sections. *Transportation Research Record: Journal of Transportation Research Board*, 1994. (1439): 25–31.
- Alobaidi, I., and Hoare, D. J. The development of pore water pressure at the subgrade-subbase interface of a highway pavement and its effect on pumping of fines. *Geotextiles and Geomembranes*, 1996. 14(2): 111–135.
- Alobaidi, I., and Hoare, D. J. Qualitative criteria for anti-pumping geocomposites. *Geotextiles and Geomembranes*, 1998. 16(4): 221–245.
- Ayres, D. J. Geotextiles or geomembranes in track? British railways' experience. *Geotextiles and Geomembranes*, 1986. 3(2–3): 129–142.
- Black, P. J., and Holtz, R. D. Performance of geotextile separators five years after installation. *Journal of Geotechnical and Geoenvironmental Engineering*, 2002. 125(5): 404–412.
- Chapuis, R. P., Contant, A., and Baass, K. A. Migration of fines in 0-20 mm crushed base during placement, compaction, and seepage under laboratory conditions. *Canadian Geotechnical Journal*, 2008. 33(1): 168–176.
- Christopher, B. R., Schwartz, C. W., and Boudreau, R. L. *Geotechnical aspects of pavements: Reference manual*. Publication FHWA NHI-05-037, FHWA, US Department of Transportation, 2006.
- Collins, B. M., Mahoney, J. P., and Holtz, R. D. FWD analysis of pavement sections with geotextile separators. Presented at Geo-Frontiers Congress, Austin, Texas, 2005.
- Currey, J. H2Ri wicking fabric experimental feature final report Dalton Highway MP 197-209 rehabilitation. Technical report, Alaska DOT&PF, Project No. IM-DP-065- 4(8)/61214. 2016.
- DeBerardino, S. J., and Baldwin, J. S. West Virginia Department of Transportation's use of a free-draining base and the role of geotextiles as long-term separators. *Geotextiles and Geomembranes*, 1996.14(3–4): 187–192.
- Dempsey, B. J. Laboratory and field studies of channeling and pumping. *Transportation Research Record: Journal of Transportation Research Board*, 1982. 849: 1–12.

- Diefenderfer, B. K., Galal, K., and Mokarem, D. W. Effect of subsurface drainage on the structural capacity of flexible pavement. Report VTRC 05-R35, Virginia Transportation Research Council, 2005.
- Grau, R. H. Engineering criteria for use of geotextile fabrics in pavement and railroad construction. Report GL-84-6, Army Engineer Waterways Experiment, Vicksburg MS Geotechnica Lab, 1984.
- Han, J. Design of planar geosynthetic-improved unpaved and paved roads. Presented at First International Symposium on Pavement and Geotechnical Engineering for Transportation Infrastructure, Nanchang, China, 2013.
- Hansen, E. C., Johannesen, R., and Armaghani, J. M. Field effects of water pumping beneath concrete pavement slabs. *Journal of Transportation Engineering*, 1991. 117(6): 679–696.
- Holtz, R. D., Christopher, B. R., and Berg, R. R. Geosynthetic design & construction guidelines: reference manual. Publication FHWA NHI-07-092, FHWA, U.S. Dept. of Transportation, 2008.
- Huang, J., Su, Q., Wang, W., Wang, X., and Guo, H. Vibration behavior and reinforcement effect analysis of the slab track-subgrade with mud pumping under cyclic dynamic loading: Full-scale model tests. *Shock and Vibration*, 2018. 2018: 1–14.
- Hufenus, R., Rueegger, R., Banjac, R., Mayor, P., Springman, S. M., and Brönnimann, R. Full-scale field tests on geosynthetic reinforced unpaved roads on soft subgrade. *Geotextiles and Geomembranes*, 2006. 24(1): 21–37.
- Kermani, B., Xiao, M., Stoffels, S. M., and Qiu, T. Magnitude and rate of migration of fine subgrade soil into granular subbase under scaled flexible interstate pavement. Presented at IFCEE 2018, Orlando, Florida, 2018a.
- Kermani, B., Xiao, M., Stoffels, S. M., and Qiu, T. Reduction of subgrade fines migration into subbase of flexible pavement using geotextile. *Geotextiles and Geomembranes*, 2018b. 46(4): 377–383.
- Koerner, R. M., and Koerner, G. R. Lessons learned from geotextile filter failures under challenging field conditions. *Geotextiles and Geomembranes*, 2015. 43(3): 272–281.
- Lin, C., Presler, W., Zhang, X., Jones, D., and Odgers, B. Long-term performance of wicking fabric in Alaskan pavements. *Journal of Performance of Constructed Facilities*, 2016. 31(2): D4016005.
- Lin, C., and Zhang, X. Laboratory Drainage performance of a new geotextile with wicking fabric. *Journal of Materials in Civil Engineering*, 2018a. 30(11): 04018293.
- Lin, C., Zhang, X., and Han, J. Comprehensive material characterizations of pavement structure installed with wicking fabrics. *Journal of Materials in Civil Engineering*, 2018b. 31(2): 04018372.

- Loulizi, A., Al-Qadi, I. L., Bhutta, S. A., and Flintsch, G. W. Evaluation of geosynthetics used as separators. *Transportation Research Record: Journal of the Transportation Research Board*, 2007. 1687(1): 104–111.
- Miszkowska, A., Lenart, S., Koda, E., Miszkowska, A., Lenart, S., and Koda, E. Changes of permeability of nonwoven geotextiles due to clogging and cyclic water flow in laboratory conditions. *Water*, 2017. 9(9): 660.
- Snaith, M. S., and Bell, A. L. The filtration behaviour of construction fabrics under conditions of dynamic loading. *Geotechnique*, 1978. 28(4): 466–468.
- Tosti, F., and Benedetto, A. Pavement pumping prediction using ground penetrating radar. *Procedia - Social and Behavioral Sciences*, 2012. 53: 1044–1053.
- Van Wijk, A. J., and Lovell, C. W. Prediction of subbase erosion caused by pavement pumping. *Transportation Research Record: Journal of the Transportation Research Board*, 1986. 45–57.
- Xiao, Y., Tutumluer, E., and Wilde, W. J. Open-graded aggregate base (OGAB) controlling subsurface moisture regime and structural stability from MnROAD instrumentation data. *T& DI Congress 2014, Orlando, Florida*, 2014.
- Yang, C., and Yu, X. Mud-pumping prevention of railway subgrade by using geotextile. Presented at the Tenth International Conference on Soil Mechanics and Foundation Engineering, Stockholm, Sweden, 1989.
- Zhang, X., and Belmont, N. Use of Mirafi nylon wicking fabric to help prevent frost heaving in Alaska pavement: 1st, 2nd, 3rd, 4th and 5th progress reports. Progress reports to TENCATE GEOSYNTHETICS (North America), 2009.
- Zhang, X., and Presler, W. Use of H2Ri wicking fabric to prevent frost boils in the Dalton Highway Beaver Slide Area, Alaska. Alaska Department of Transportation and Public Facilities. 2012.
- Zuo, G., Drumm, E.C., Meier, R.W., Randy Rainwater, N., Marshall, C., Wright, W.C., and Yoder, R.E. Observed long-term water content changes in flexible pavements in a moderate climate. In *Proceedings of the Geotechnical Special Publication*; 2004; pp. 1066–1075.